Journal of Autoimmunity 99 (2019) 81–97

Contents lists available at ScienceDirect

Journal of Autoimmunity

journal homepage: www.elsevier.com/locate/jautimm

Counter-regulation of regulatory T cells by autoreactive CD8$^+$ T cells in rheumatoid arthritis

Ilenia Cammarata[a,1], Carmela Martire[a,1], Alessandra Citro[a], Domenico Raimondo[b], Doriana Fruci[c], Ombretta Melaiu[c,d], Valentina D'Oria[e], Chiara Carone[f], Giovanna Peruzzi[g], Cristina Cerboni[b,h], Angela Santoni[b,g,h], John Sidney[i], Alessandro Sette[i], Marino Paroli[j], Rosalba Caccavale[j], Edoardo Milanetti[k], Mara Riminucci[b], Eleonora Timperi[a], Silvia Piconese[a,h], Antonio Manzo[l], Carlomaurizio Montecucco[l], Rossana Scrivo[a], Guido Valesini[a], Elisabetta Cariani[f], Vincenzo Barnaba[a,g,h,*]

[a] Dipartimento di Medicina Interna e Specialità Mediche, Sapienza Università di Roma, 00161, Rome, Italy
[b] Dipartimento di Medicina Molecolare, Sapienza Università di Roma, 00161, Rome, Italy
[c] Dipartimento di Ematologia/Oncologia, Ospedale Pediatrico Bambino Gesù, IRCCS, 00165 Rome, Italy
[d] Dipartimento di Biologia, Università di Pisa, 56126, Pisa, Italy
[e] Core Facility Research Laboratories, Ospedale Pediatrico Bambino Gesù, IRCCS, 00165, Rome, Italy
[f] Ospedale Civile S. Agostino-Estense, 41126, Modena, Italy
[g] Center for Life Nano Science@Sapienza, Istituto Italiano di Tecnologia, 00161, Rome, Italy
[h] Istituto Pasteur - Fondazione Cenci Bolognetti, 00185, Rome, Italy
[i] La Jolla Institute for Allergy and Immunology, San Diego, CA, 92121, USA
[j] Dipartimento di Scienze e Biotecnologie Medico-Chirurgiche, Sapienza Università di Roma, Polo Pontino, 04100, Latina, Italy
[k] Dipartimento di Fisica, Sapienza Università di Roma, 00185, Rome, Italy
[l] Dipartimento di Medicina Interna e Terapia Medica, Fondazione IRCCS Policlinico "San Matteo", Università di Pavia, 27100, Pavia, Italy

ARTICLE INFO

Keywords:
Rheumatoid arthritis
Autoreactive CD8$^+$ T cells
Regulatory T cells
Counter-regulation

ABSTRACT

The mechanisms whereby autoreactive T cells escape peripheral tolerance establishing thus autoimmune diseases in humans remain an unresolved question. Here, we demonstrate that autoreactive polyfunctional CD8$^+$ T cells recognizing self-antigens (i.e., vimentin, actin cytoplasmic 1, or non-muscle myosin heavy chain 9 epitopes) with high avidity, counter-regulate Tregs by killing them, in a consistent percentage of rheumatoid arthritis (RA) patients. Indeed, these CD8$^+$ T cells express a phenotype and gene profile of effector (eff) cells and, upon antigen-specific activation, kill Tregs indirectly in an NKG2D-dependent bystander fashion *in vitro*. This data provides a mechanistic basis for the finding showing that AE-specific (CD107a$^+$) CD8$^+$ T killer cells correlate, directly with the disease activity score, and inversely with the percentage of activated Tregs, in both steady state and follow-up studies *in vivo*. In addition, multiplex immunofluorescence imaging analyses of inflamed synovial tissues *in vivo* show that a remarkable number of CD8$^+$ T cells express granzyme-B and selectively contact FOXP3$^+$ Tregs, some of which are in an apoptotic state, validating hence the possibility that CD8$^+$ Teff cells can counteract neighboring Tregs within inflamed tissues, by killing them. Alternatively, the disease activity score of a different subset of patients is correlated with the expansion of a peculiar subpopulation of autoreactive low

Abbreviations: TCRs, T cell receptors; Treg, regulatory T cell; N, naïve; eff, effector; VIME, vimentin; ACTB, actin cytoplasmic 1; MYH9, non-muscle myosin heavy chain 9; AE, apoptotic epitope; HDs, healthy donors; DCs, dendritic cells; L, ligand; RA, rheumatoid arthritis; TNF, tumor necrosis factor; NRs, non-responders; Rs, responders; ACR, American College of Rheumatology; DMARDs, disease-modifying anti-rheumatic drugs; DAS28, Disease Activity Score 28 joints; EULAR, European League Against Rheumatism; R, receptor; SF, synovial fluid; MFI, mean fluorescence intensity; IHC, immunohistochemical; IF, immunofluorescence; CMV, cytomegalovirus; FITC, fluorescein isothiocyanate; PI, propidium iodide; EM, effector memory; EMRA, effector memory RA$^+$; APC, allophycocyanin; FSC-A, forward scatter area; SSC-A, side scatter area; CTLA-4, Cytotoxic T-Lymphocyte Antigen-4; PD-1, programmed death-1; IFN, interferon; p, phosphorylated; GZM, granzyme; CFSE, carboxyfluorescein succinimidyl ester; FC, flow cytometry; NKG2D, NK group 2 member D; MTE, Multiplexed Target Enrichment; N-HDs, naïve in healthy donors; N-Ps, naïve in patients; Eff-HDs, effector cells in healthy donors; Eff-Ps, effector cells in patients; CDF, cumulative distribution function; PCA, principal component analysis; RF, rheumatoid factor; ACPA, anti-citrullinated protein antibody; CRP, C reactive protein; ESR, erythrocyte sedimentation rate; Eomes, Eomesodermin; T-bet, transcription factor T-box; CB, cord blood; pa, partially activated; TMNP, memory T cells with a naive phenotype; act, activated

* Corresponding author. Dipartimento di Medicina Interna e Specialità Mediche, Sapienza Università di Roma, 00161, Rome, Italy.
E-mail address: vincenzo.barnaba@uniroma1.it (V. Barnaba).
[1] These authors contributed equally to this work.

https://doi.org/10.1016/j.jaut.2019.02.001
Received 7 January 2019; Received in revised form 5 February 2019; Accepted 5 February 2019
Available online 16 February 2019

avidity, partially-activated (pa)CD8$^+$ T cells that, despite they conserve the conventional naïve (N) phenotype, produce high levels of tumor necrosis factor (TNF)-α and exhibit a gene expression signature of a progressive activation state. Tregs directly correlate with the expansion of this autoreactive (low avidity) paCD8$^+$ TN cell subset *in vivo*, and efficiently control their differentiation rather their proliferation *in vitro*. Interestingly, autoreactive high avidity CD8$^+$ Teff cells or low avidity paCD8$^+$ TN cells are significantly expanded in RA patients who would become non-responders or patients who would become responders to TNF-α inhibitor therapy, respectively. These data provide evidence of a previously undescribed role of such mechanisms in the progression and therapy of RA.

1. Introduction

The central mechanism of T cell tolerance in the thymus does not impede a huge number of autoreactive T cells (i.e., those with low affinity/avidity T cell receptors [TCRs]) from migrating to the periphery [1–3]. Therefore, additional mechanisms of tolerance are required to avoid autoimmunity in the periphery [4], including the emergence of functional regulatory T cells expressing the X-linked transcription factor FOXP3 (Tregs) [5,6]. Tregs can prevent the differentiation of autoreactive T naïve (N) cells into detrimental effector (eff) cells, or limit the excessive immunopathology by Teff cells, through a wide range of immunosuppressive mechanisms [7,8]. In addition, Tregs maintain self-tolerance by inducing anergy of autoreactive TN cells in healthy individuals [9]. How autoreactive Teff cells can escape Treg control establishing thus autoimmune diseases in humans, however, remains an open question.

To address this issue, we built on our previous research demonstrating the presence of autoreactive CD8$^+$ T cells specific to a wide repertoire of self-antigenic determinants derived from apoptotic T cells (including vimentin [VIME], actin cytoplasmic 1 [ACTB], and non-muscle myosin heavy chain 9 [MYH9], from this point onward referred to apoptotic epitopes [AEs]) in both healthy donors (HDs) and (to a significantly higher extent) in patients with various forms of chronic inflammatory diseases [10–14]. AE-specific CD8$^+$ T cells are induced as a result of cross-priming by CD40$^+$ dendritic cells (DCs) that had previously phagocytosed CD40 ligand (CD40L)$^+$ apoptotic T cells (in turn derived from CD40L$^+$ activated T cells infiltrating inflamed tissues), processed caspase-cleaved cellular proteins, and cross-presented the resulting AEs on MHC class I molecules [13,15–18].

Rheumatoid arthritis (RA) is a prototypical human autoimmune disease principally characterized by severe and destructive inflammatory polyarthritis [19]. Complex interactions among genetic, immunologic, and environmental factors play a role in RA development [19–24]. Clinical evidence showed that various therapeutic antibodies neutralizing inflammatory cytokines (e.g., tumor necrosis factor [TNF]-α, IL-1, IL-6, IL-17) or blocking some related receptors benefit a significant percentage of patients [19,25,26]. In particular, anti-TNF therapies have revolutionized the disease progression and cure of RA [19,25,26]. However, 20%–40% RA patients result non-responders (NRs) to therapy with any anti-TNF-α reagent [25]. Since both patients who become responders (Rs) and those resulting NRs show similar disease activity scores and duration of disease before the start with this therapy, it is reasonable to hypothesize that divergent immunoregulatory mechanisms may contribute to the development of the R or NR state. AE-specific CD8$^+$ T cells correlate with RA progression and have been proposed to represent a unique predictive biomarker discriminating patients who become Rs or NRs following TNF-α inhibitor therapies [10]. The spreading of these responses can amplify immunopathology [10,11,13–18], likely as a consequence of a primary (i.e., self- or pathogen-specific) immune response initiating RA [27,28]. Autoantibodies to both native and citrullinated forms of some of these cellular proteins represent the master biomarkers of autoimmunity in RA [29,30].

In this study, we provide evidence both for the molecular mechanisms licensing AE-specific CD8$^+$ Teff cells to be resistant to Treg suppression, and for their impact in the progression and therapy of RA.

2. Material and methods

2.1. Study population

Fifty-one HLA-A2$^+$ biologic-naïve RA (in accordance with the 1987 American College of Rheumatology [ACR] criteria) patients, who had shown an unsatisfactory response to conventional disease-modifying antirheumatic drugs (DMARDs) including methotrexate (associated or not associated with other anti-inflammatory/immunosuppressive drugs), were included in the study (Table 1). 39 patients were submitted to subsequent treatment with etanercept (50 mg per week), and 12 with adalimumab (40 mg every other week), in association with methotrexate. Clinical response was set as an improvement of the Disease Activity Score 28 joints (DAS28) $>$ 0.6 (moderate response) after four months of therapy in accordance with the European League Against Rheumatism (EULAR) response criteria [31,32]. Of 51 patients, 33 would become Rs and 18 NRs to anti-TNF therapies (Table 1). 33 patients were enrolled in the Dipartimento di Medicina Interna e Specialità Mediche – Sapienza Università di Roma: PBMCs from these patients were used for the majority of analyses. The remaining 18 patients were enrolled in the Dipartimento di Scienze e Biotecnologie Medico-Chirurgiche – Sapienza Università di Roma. The latter were enrolled

Table 1
Demographic and clinical characteristics of enrolled RA patients.

	All	Responders[a]	Non-responders[a]
Number of patients	51	33/51	18/51
Gender F/M	45/6	29/4	16/2
Age, years *range*	57.5 36–84	55.2 36–84	60.6 39–77
Disease duration, months *range*	96.4 6–300	88.6 6–240	107.8 9–300
ESR (T0) *range*	25.6 2–78	26.1 2–62	25.1 5–78
CRP (mg/dl) (T0) *range*	1.0 0–1.4	1.0 0–1.2	0.9 0.14–1.4
DAS28-ESR ± SD (T0) *range*	4.8 ± 1.1 1.26–7.1	4.8 ± 1.3 1.26–7.1	4.7 ± 0.9 2.9–6.1
DAS28-CRP ± SD (T0) *range*	4.3 ± 1.3 2.3–8.3	4.2 ± 1.4 2.3–7.0	4.3 ± 1.1 2.9–8.3
DAS28-ESR ± SD (T4) *range*	3.4 ± 1.2 0.49–5.51	2.9 ± 0.9 0.49–4.45	4.2 ± 1.1 1.99–5.51
DAS28-CRP ± SD (T4) *range*	3.2 ± 1.6 1.03–7.5	2.4 ± 1.6 1.03–4.20	4.1 ± 1.4 2.36–7.5
RF (pos/neg/ND)	31/14/6	22/7/4	9/7/2
ACPA (pos/neg/ND)	29/14/8	21/8/4	8/6/4
HAQ (T0)	1.0	0.9	1.1
Etanercept	39	24	15
Adalimumab	12	9	3

T0 = time before the start of treatment with biological disease-modifying antirheumatic drugs (bDMARDs; etanercept or adalimumab); **T4** = time after 4 months of treatment with bDMARDs; **ESR** = erytrocyte sedimentation rate; **CRP** = C-reactive protein; **DAS28** = Disease Activity Score in 28 joints; **RF** = rheumatoid factor; **ACPA** = anti-citrullinated protein antibodies; **HAQ** = health assessment questionnaire; **SD** = standard deviation; **ND** = not detected.

[a] Patients who develop into Responders or Non-responders to TNF-α inhibitor therapies.

later for analyzing correlations between AE-specific $CD8^+$ T cells producing TNF-α in response to relevant epitopes and TNF receptor (R)2^+ Tregs (see Fig. 5D and E), or between AE-specific $CD8^+$ T cells expressing CD107a in response to relevant epitopes and actTregs, for the longitudinal analyses during the course of anti-TNF therapy (see Fig. 8). In addition, synovial fluid (SF)-derived mononuclear cells and the corresponding PBMCs were obtained from four independent RA patients with severe disease activity at the baseline. Thirty HLA-$A2^+$ age-matched and sex-matched HDs were included in the study as controls. The immunohistochemical (IHC) and multiplex immunofluorescence (IF) analyses were performed on selected paraffin-embedded synovial tissue samples from 7 patients with severe RA obtained by Divisione di Reumatologia, Dipartimento di Medicina Interna e Terapia Medica, Fondazione IRCCS Policlinico "San Matteo", Università di Pavia. All patients and donors provided written informed consent before sampling, in accordance with the Declaration of Helsinki, and the study protocol was approved by the Sapienza Università di Roma – Azienda Policlinico Umberto I research ethics committee (n.3202/15.05.2014).

2.2. Synthetic peptides

The synthetic peptides $MYH9_{478\text{-}486}$ (QLFNHTMFI), $MYH9_{741\text{-}749}$ (VLMIKALEL), $VIME_{78\text{-}87}$ (LLQDSVDFSL), $VIME_{225\text{-}233}$ (SLQEEIAFL), or $ACTB_{266\text{-}274}$ (FLGMESCGI), were prepared based on the sequence of caspase-cleaved proteins that had been identified by the proteomic analyses of apoptotic T cells, as described previously [13]. All the peptides were synthesized and selected for their capacity to bind the HLA-A2 molecule [13]. The cytomegalovirus (CMV)pp65 (NLVPMVATV) peptide was purchased from Chi Scientific (Maynard, USA).

2.3. Cell preparation, purification, and sorting

PBMCs were isolated from fresh heparinized blood by density gradient centrifugation with Lympholyte (Cedarlane, Burlington, Canada) and collected in complete RPMI medium containing 10% heat-inactivated FBS (HyClone GE Healthcare Life Sciences, Utah, USA), 2 mM L-glutamine (Sigma-Aldrich, St. Louis, MO), penicillin/streptomycin (EuroClone, Milan, Italy), non-essential amino acids (EuroClone), and sodium pyruvate (EuroClone). Similarly, MNCs were isolated from SFs. Spontaneous apoptosis of T cells was determined by staining fresh PBMCs with mAbs to CD3 and CD40L and with fluorescein isothiocyanate (FITC)-labelled Annexin V (BioLegend, San Diego, CA), and propidium iodide (PI) (antibody details reported in Table S1). Highly purified $CD8^+$ TN ($CCR7^+CD45RA^+$) cells and Tregs were isolated from HLA-$A2^+$ PBMCs by magnetic bead-separation with the Naïve $CD8^+$ T Cell Isolation Kit (Miltenyi Biotec, Bergisch Gladbach, Germany) and the $CD4^+CD25^+$ Regulatory T Cell Isolation Kit (Miltenyi Biotec), respectively. The combination of highly purified $CD8^+$ T effector memory (EM; $CCR7^-CD45RA^-$) and effector memory RA^+ (EMRA; $CCR7^-CD45RA^+$) cell population was obtained by using the positive fraction after enrichment of $CD8^+$ TN cells. Each purified cell subset was used in the various experiments only when the purity of the corresponding cells was > 96% and 90% for $CD8^+$ T cell populations and Tregs, respectively. To sort AE-specific $CD8^+$ TN or EM + EMRA cells used for gene-expression profile determination, $CD8^+$ T cells were pre-enriched from PBMCs of patients and HDs with the $CD8^+$ T Cell Isolation Kit (Miltenyi Biotec), stained with Fixable Viability Dye eFluor780 (eBioscience, Massachusetts, USA), the pool of allophycocyanin (APC)-labelled-HLA-A*0201 dextramers complexes to AEs and mAbs to CD8, CD45RA, and CCR7, and a dump channel, as described previously (antibody details reported in Table S1). After 20 min at 4 °C, cells were washed, resuspended in PBS containing 2%FBS and sorted using a FACSAria III (BD Biosciences, San Jose, CA) equipped with 488 nm, 561 nm and 633 nm laser and FACSDiva software (BD Biosciences version 6.1.3). Data were analyzed using FlowJo software (Tree Star, San Carlos, CA). Briefly, cells first gated based on forward and side scatter area (FSC-A and SSC-A) plot to identify the population and doublets exclusion by plotting the width against the area of FSC and SSC parameters, were then detected for specific fluorochromes in order to obtain Naïve ($CD45RA^+CCR7^+$) and EM + EMRA ($CD45RA^{-/+}CCR7^-$) subsets from both the dextramer-positive and dextramer-negative fractions. Following isolation, an aliquot of tubes of the collected cells was evaluated for purity at the same sorter resulting in an enrichment > 98–99% for each sample.

2.4. HLA class I dextramer/peptide complexes and antibodies

PBMCs were first stained with Fixable Viability Dye eFluor780 for the exclusion of dead cells (PBS, 30 min at room temperature). After washing, cells were incubated with the pool of APC-labelled-HLA-A*0201 dextramers complexed with $MYH9_{478\text{-}486}$ (QLFNHTMFI), $MYH9_{741\text{-}749}$ (VLMIKALEL), $VIME_{78\text{-}87}$ (LLQDSVDFSL), $VIME_{225\text{-}233}$ (SLQEEIAFL), or $ACTB_{266\text{-}274}$ (FLGMESCGI) peptides, as well as with APC-labelled-HLA-A*0201 dextramers complexed with the cytomegalovirus $(CMV)_{pp65}$ (NLVPMVATV) peptide (IMMUDEX, Copenhagen, Denmark). A negative control dextramer, conjugated to irrelevant peptide (ALIAPVHAV), was used (Immudex) to set up the dextramer-positive gate. The incubation was performed in PBS containing 2% FBS at room temperature for 10 min. After washing multiparametric surface staining was performed, which involved incubating the cells with the labelled mAbs to CD8, CD45RA, CCR7, CD11a, HLA-DR, CD62L, CD69, CD95, Cytotoxic T-Lymphocyte Antigen (CTLA)-4, and programmed death (PD)-1, and with a cocktail of labelled mAbs to CD14, CD16, CD56, CD19, and with Fixable Viability Dye eFluor 780 (dump channel was included for the exclusion of monocytes, NK cells, and B cells, respectively; antibody details reported in Table S1) for 20 min at 4 °C. Cells were acquired with LSRFortessa cytometer (BD Biosciences) and analyzed with FlowJo software version 10.0.8r1 (Tree Star, San Carlos, CA).

2.5. Intracellular staining

PBMCs were incubated with or without the peptides (20 μg/mL of AE pool or 10 μg/mL of CMV peptide) plus anti-CD28 mAb (1 μg/mL) (BD Biosciences) and the Protein Transport Inhibitor Cocktail (Brefeldin A and Monensin; eBioscience), or with the Cell Stimulation plus Protein Transport Inhibitor Cocktail (eBioscience) as a positive control, and mAb to CD107a for degranulation analysis, for 6 h at 37 °C. After antigen stimulation, cells were washed and stained with Fixable viability Dye (eFluor780), the pool of APC-labelled-HLA-A*0201 dextramers complexed with the corresponding peptides, followed by surface staining with mAbs to CD8, CD45RA, and CCR7, and the dump channel as reported previously (antibody details reported in Table S1). Cells were fixed and permeabilized using the BD Cytofix/Cytoperm Fixation/Permeabilization Solution Kit (BD Biosciences) at 4 °C for 20 min, washed, and stained with mAbs to interferon (IFN)-γ and TNF-α (BD Perm/Wash buffer, BD Biosciences) for 20 min at 4 °C. For phosphorylated (p)ZAP70 staining, cells (following antigen stimulation as described previously), were stained with the pool of APC-labelled-HLA-A*0201 dextramers, fixed with BD Cytofix/Cytoperm Fixation/Permeabilization Solution Kit (BD Biosciences) at 4 °C for 20 min, and then underwent surface staining with mAbs to CD8, CD45RA, and CD27, and the dump channel as reported previously (antibody details reported in Table S1). Next, cells were treated with pre-chilled Phospho Flow Perm Buffer III (BD Biosciences) for 30 min at 4 °C, and stained with mAb to pZAP70 (antibody details reported in Table S1) in PBS containing 2% FCS for 30 min at room temperature. Tregs were analyzed by surface staining with mAbs to CD4, CD127, CD25, and CD45RA, fixation and permeabilization (FOXP3/Transcription Factor Staining Buffer Set; eBioscience) and subsequent intra-nuclear staining with mAb to FOXP3 (antibody details reported in Table S1). Cells were washed, acquired with an LSRFortessa cytometer, and analyzed with FlowJo software

version 10.0.8r1 (Tree Star). For the evaluation of intra-nuclear molecules (after surface staining), unstimulated PBMCs were fixed and permeabilized with the FOXP3/Transcription Factor Staining Buffer Set in accordance with the manufacturer's instructions. Upon washing, cells were stained with anti-human mAbs to Eomes, T-bet, and Ki67 (antibody details reported in Table S1), and diluted in the eBioscience permeabilization buffer for 30 min at room temperature. Following surface staining, stainin with mAb to granzyme (GZM)B (antibody details reported in Table S1) was performed with the Cytofix/Cytoperm Fixation/Permeabilization Solution Kit (BD Biosciences). Cells expressing cytokines or nuclear molecules were analyzed in $CD8^+$dextramer$^+$ cells after exclusion of B cells, monocytes, natural killer T cells, NK cells, and $CD4^+$ T cells (dump channel).

2.6. Suppression assays

Highly purified autologous $CD8^+$ TN cells were labelled with 10 μM of carboxyfluorescein succinimidyl ester (CFSE) (Thermo Fisher Scientific, Massachusetts, USA) for 15 min at 37 °C. Then, they were co-cultured with both autologous γ-irradiated (70Gy) PBMCs as APCs (at a 1:1 ratio), which had previously been pulsed or not with 20 μg/mL of AE pool plus 1 μg/mL of anti-CD28 mAb, and highly purified Tregs, which had previously been stained with 5 μM of CellTrace Violet (Cell Proliferation Kit, Thermo Fisher Scientific) at different CD8:Treg ratios (100:1, 10:1, 4:1, and 1:0), in RPMI complete medium containing 5% human serum AB, in 96-well plate (round bottom). Cells were cultured for 7 days, and half of the medium was replaced with fresh medium containing 20 IU/mL of IL-2 at day 4. In parallel, the same experiment was performed with highly purified $CD8^+$ TEM + EMRA cells by using the positive fraction after enrichment of $CD8^+$ TN cells. Cells were stained with Fixable Viability Dye eFluor780, dextramers and mAbs to CD8, CD4, CCR7, CD45RA and FOXP3 as reported previously (antibody details reported in Table S1). The same experiment was performed with CMV-pp65 (NLVPMVATV) $CD8^+$ T cells. The percentage of Treg-mediated suppression was calculated using the following formula: %Treg suppression = (MFI CFSE-stained AE-$CD8^+$ T cells with Tregs – CFSE-stained AE-$CD8^+$ T cells without Tregs)/(MFI CFSE-stained AE-$CD8^+$ T cells with Tregs) x 100.

2.7. Flow cytometry (FC)-based bystander killing assay

Highly purified $CD8^+$ TEM + EMRA or TN cells were stained with 10 μM of CFSE and co-cultured with autologous γ-irradiated (70Gy)-PBMCs (1:1 ratio), which had previously been pulsed (or not) with 20 μg/mL of AE pool plus 1 μg/mL of anti-CD28, and highly purified allogeneic (HLA-A2$^-$) Tregs, which had previously been stained with 5 μM of CellTrace Violet (CellTrace Cell Proliferation Kit). $CD8^+$ T cells and Tregs were co-cultured (or not) at a ratio of 10:1 for 7 days in complete RPMI medium containing 5% human serum AB; at day 3, half of the medium was replaced with fresh medium plus 20 IU/mL of IL-2. To investigate the GZMB-mediated killing effect of $CD8^+$ TEM + EMRA on Tregs, we performed the assays in the presence of GZMB inhibitor (Santa Cruz Biotechnology, Dallas, USA) or NK group 2 member D (NKG2D) neutralizing Ab (R&D Systems, Minneapolis, USA). Specifically, Tregs were treated (or not) with 20 μM of GZMB inhibitor for 1 h at 37 °C, and $CD8^+$ TEM + EMRA cells were treated with 1 μg/1 × 10^6 of NKG2D neutralizing Ab for 15 min at room temperature. Cells were then stained, as reported previously.

2.8. FC-based direct killing assay

Highly purified $CD8^+$ T cells were co-cultured with autologous γ-irradiated (70Gy)-PBMCs (1:1 ratio) as APCs, which had previously been pulsed (or not) with 20 μg/mL of AE pool plus 1 μg/mL, in complete RPMI medium containing 5% human serum AB. After 3 days half of the cell culture medium was replaced with fresh medium plus 50 IU/mL of IL2 after 3 days. After 6 days, $CD8^+$ T EM + EMRA cells, used as effector (E) cells, were enriched by magnetic bead separation, as described previously, and purity of enriched cells (> 96%) was checked with an LSRFortessa cytometer. Highly purified autologous Tregs were used as target (T) cells (purity ≥90%). Tregs were separated and stained with two different concentrations of CFSE: 10 μM ($CFSE^{high}$) or 0.5 μM ($CFSE^{low}$). Only the $CFSE^{low}$ fraction was pulsed for 45 min with 20 μg/mL of AE pool at 37 °C. CFSE high and low fractions were mixed at a 1:1 ratio and seeded in co-culture with pre-activated $CD8^+$ TEM + EMRA cells [33] at different ratios (10:1, 5:1, 1:1, 0.1:1, 0:1), keeping the number of target cells fixed. After co-culturing for 6 h at 37 °C, cells were stained with Fixable Viability Dye eFluor780 for the enumeration of dead cells. After washing, cells were incubated with the pool of dextramers complexed with AE, and stained with mAbs to CD8, CD4, CD127 and FOXP3, as described previously. The percentage of specific killing was calculated using the formula: %specific killing = 1 – [MFI ($CFSE^{low}$/$CFSE^{high}$) with E/($CFSE^{low}$/$CFSE^{high}$) without E] x 100. To investigate the involvement of GZMB in direct killing, target cells were treated with 20 μM of GZMB inhibitor for 1 h at 37 °C before CFSE staining.

2.9. Nanostring

The RNeasy Plus Micro Kit (Qiagen, Hilden, Germany) was used to extract RNA from 130 sorted cells from all samples. Samples were stored at −80 °C until the assays were performed. Gene expression profiling was carried with the nCounter® Single Cell Human Immunology v2 Kit (Nanostring Technologies, Washington, USA) which relies on the Multiplexed Target Enrichment (MTE) system. The use of MTE primers enables specific and linear enrichment of up to 800 targets in a single sample. The nCounter® Single Cell Human Immunology v2 Kit contains fluorescent barcoded probes that are complementary to both 571 immune-response and inflammation–associated genes, and 13 housekeeping genes (used as internal controls). Moreover, it provides 8 negative controls and 6 positive controls at different concentrations, so as to check the performance of each experiment and to correct any differences in preparation, hybridization and reagent dispensation. In accordance with the experimental protocol, 4 μL of total RNA was incubated with 1 μL of SuperScript VILO Master Mix (Invitrogen, Life Technologies, Carlsbad, CA) at 25 °C for 10 min, then at 42 °C for 60 min, and finally at 85 °C for 5 min to perform RNA reverse transcription. Then, cDNA was denaturated at 94 °C for 10 min and, after the addition of 1 μL of pooled MTE primers and 5 μL of TaqMan Pre Amp Master Mix (Applied Biosystems, Life Technology), amplified by 18 PCR cycles at 94 °C for 15 s and 60 °C for 4 min. After denaturation (94 °C for 2 min, then on ice), the amplification product was hybridized for 18 h at 65 °C in the presence of both reporter and capture probes. The nCounter Prep Station was then used to purify and immobilize the resulting hybrid onto the internal surface of a cartridge. To quantify mRNA targets, each cartridge was scanned in 550 field-of-view by means of the automatic nCounter Digital Analyzer. To perform gene expression analysis, raw count data were preprocessed with the NanoStringNorm R package [34], a set of tools for normalizing, running diagnostics, and visualizing NanoString nCounter data. Specifically, geometric mean-based scaling normalization was performed to account for technical assay variation, which involved choosing the “geo.mean” setting in the CodeCount R option. The background subtracted from each sample was calculated by setting “mean.2 s d” in the background option. The method used to normalize for RNA content (i.e., pipetting fluctuations) entailed selecting the “housekeeping.geo.mean” setting in the Sample Content R option via all internal annotated housekeeping genes. All data were grouped in four classes based on cell sample subtype: naïve in healthy donors (N-HDs), naïve in patients (N-Ps), effector cells in healthy donors (Eff-HDs), and effector cells in patients (Eff-Ps). We did not consider genes that are not expressed in any sample, thereby excluding them from further analysis. This resulted in

an analysis set of 401 unique genes and 26 samples. Finally, normalized data were log2 transformed and used for downstream analyses. The expression profiles (in NanoString counts) of relevant gene sets were analyzed through heat-map representation. To perform cluster analysis, we chose the hierarchical agglomerative clustering procedure, which has a bottom-up approach. This procedure involved using Ward's method and a Euclidean distance metric. Ward's method, essentially, looks at cluster analysis as an analysis of variance problem, starting out with n clusters of size 1 and continuing until all the observations are included into one cluster. Hierarchical clustering of samples and genes was performed with the "heatmap.2" R function by employing "gplot" and "dendextend" packages [35]. Each cell was colored to reflect quantitatively the relative expression, in NanoString counts, to assist in visualizing expression changes. We calculated the cumulative distribution function (CDF) by applying the "ecdf" R function of the "stats" library to a data sample, thereby generating a function representing the empirical CDF. The CDF indicates the probability that a random variate X takes on a value less than or equal to x. The CDF takes on values in the interval [0,1]. To test for the equality of two cumulative density functions, we performed a Kolmogorov-Smirnov test by using the "ks.test" function in R. Differences between CDF were considered significant at $p < 0.01$. Next, principal component analysis (PCA) was used to identify expression profiles that accounted for the majority of the variance (in expression) between the 26 cell subset. Our expression data set (in NanoString counts) was organized in a matrix composed by 26 columns and 401 rows where each row corresponds to a different gene and each column corresponds to one of 26 samples whose immunology-related transcripts pattern was characterized. The first three components (PC1, PC2 and PC3) account for over 60% of the variance and the first two account for 56% allowing most of the information to be visualized also in two dimensions if we consider dispersion of our data. We performed PCA by using the built-in R function prcomp.

2.10. IHC and multiplex IF staining and acquisition

IHC and IF staining were performed in 2 μm of formaldehyde-fixed paraffin embedded serial tissue sections following deparaffinization and antigen retrieval as previously described [36]. For IHC, sections were blocked with the avidin/biotin blocking system (Thermo Fisher Scientific, Fremont CA, USA) according to the manufacturer's instructions and then incubated (overnight at 4 °C) with primary antibodies (Table S1). This step was followed by incubation with secondary antibodies coupled with streptavidin alkaline phosphatase (Dako). Bound streptavidin was detected with Fast Red chromogen substrate (Dako). Tissue staining were counterstained with En Vision FLEX Haematoxylin (Dako). Sections of normal tonsils were used as positive controls. Isotype-matched mouse mAbs were used as negative controls. Slides were analyzed using an image analysis workstation (Nikon Eclipse E600). The density of $CD8^+$ and $FOXP3^+$ T cells was recorded by two blinded examiners as the number of positive cells per unit tissue surface area (mm^2). The mean of positive cells detected in 5 fields for each sample was used in the statistical analysis. For IF, slides were blocked for

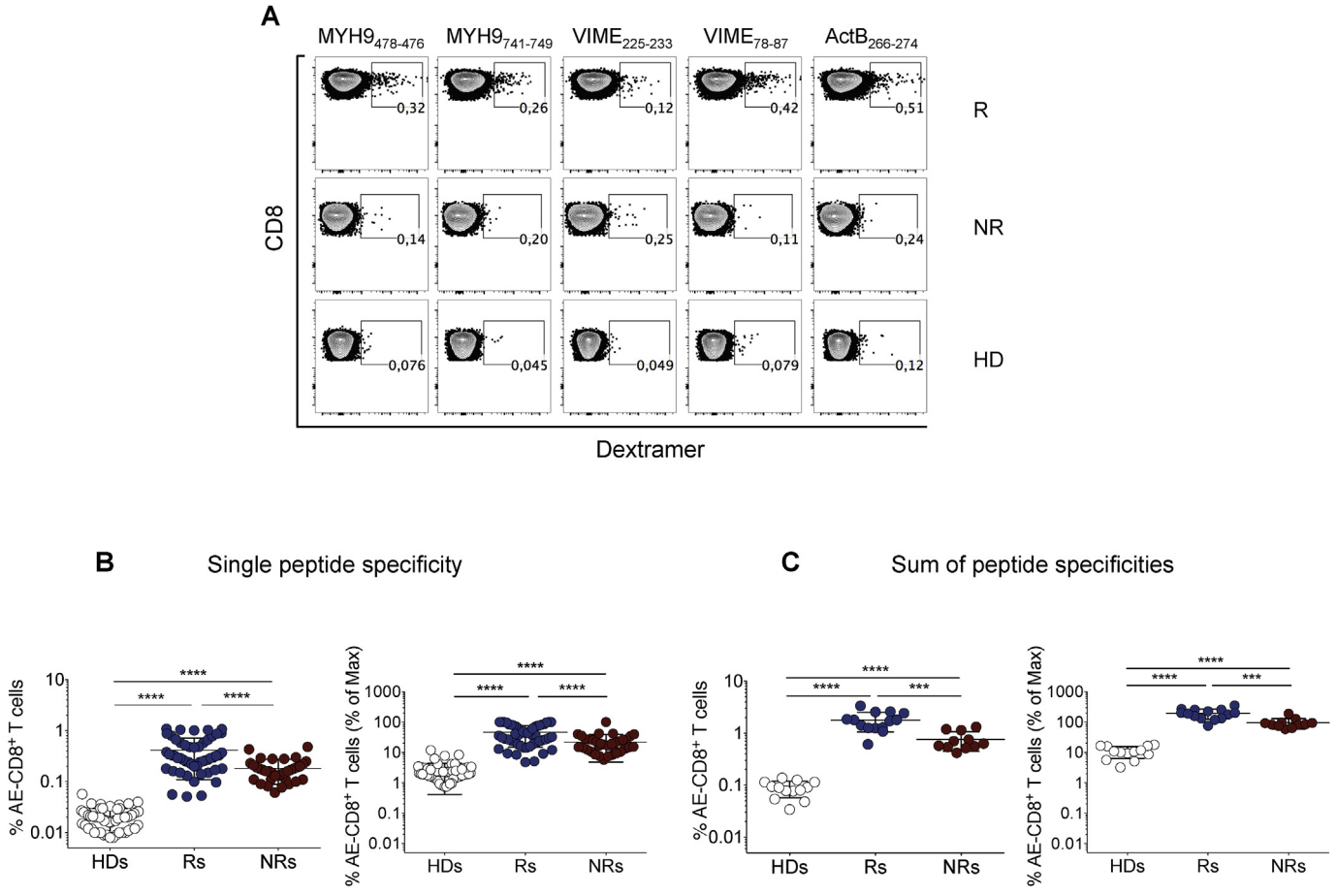

Fig. 1. AE-specific $CD8^+$ T cells in RA patients who will (or will not) benefit from anti-TNF-α therapy. (A) Representative FC analysis of dextramer$^+$$CD8^+$ T cells specific to AE in a R, a NR, or a HD. (B) Single dextramer$^+$$CD8^+$ T cells specific populations represented as percentage of dextramer$^+$ AE-specific (AE)-$CD8^+$ T cells (left graph) and percentage of maximum (% of Max) (right graph), in HDs (n = 13), Rs (n = 14) and NRs (n = 11) (each symbol represents response to single peptide). For each antigen, the % of Max was calculate setting the value of 100% to the maximum percentage of response, and then we normalized the other values. (C) Sum of the percentages (left graph) and sum of the percentages of maximum (right graph) of all dextramer$^+$$CD8^+$ T cells detected in a single HD or patient (each symbol is a single individual); ***$p < 0.005$, ****$p < 0.0001$ by the unpaired *t*-test.

60 min with 1% BSA and 5% normal goat serum and then each antibody was added consecutively as follows. First, sections were incubated with anti-FOXP3 Ab overnight at 4 °C, followed by 60 min incubation with Alexa Fluor 488 goat anti-mouse IgG. Next, slides were incubated with anti-cleaved Caspase-3 overnight at 4 °C, followed by 60 min incubation with Alexa Fluor 594 goat anti-rabbit IgG. Finally, slides were incubated with DyLight 550 anti-Granzyme overnight at 4 °C, followed by 40 min incubation with mouse IgG and then 60 min with Alexa Fluor

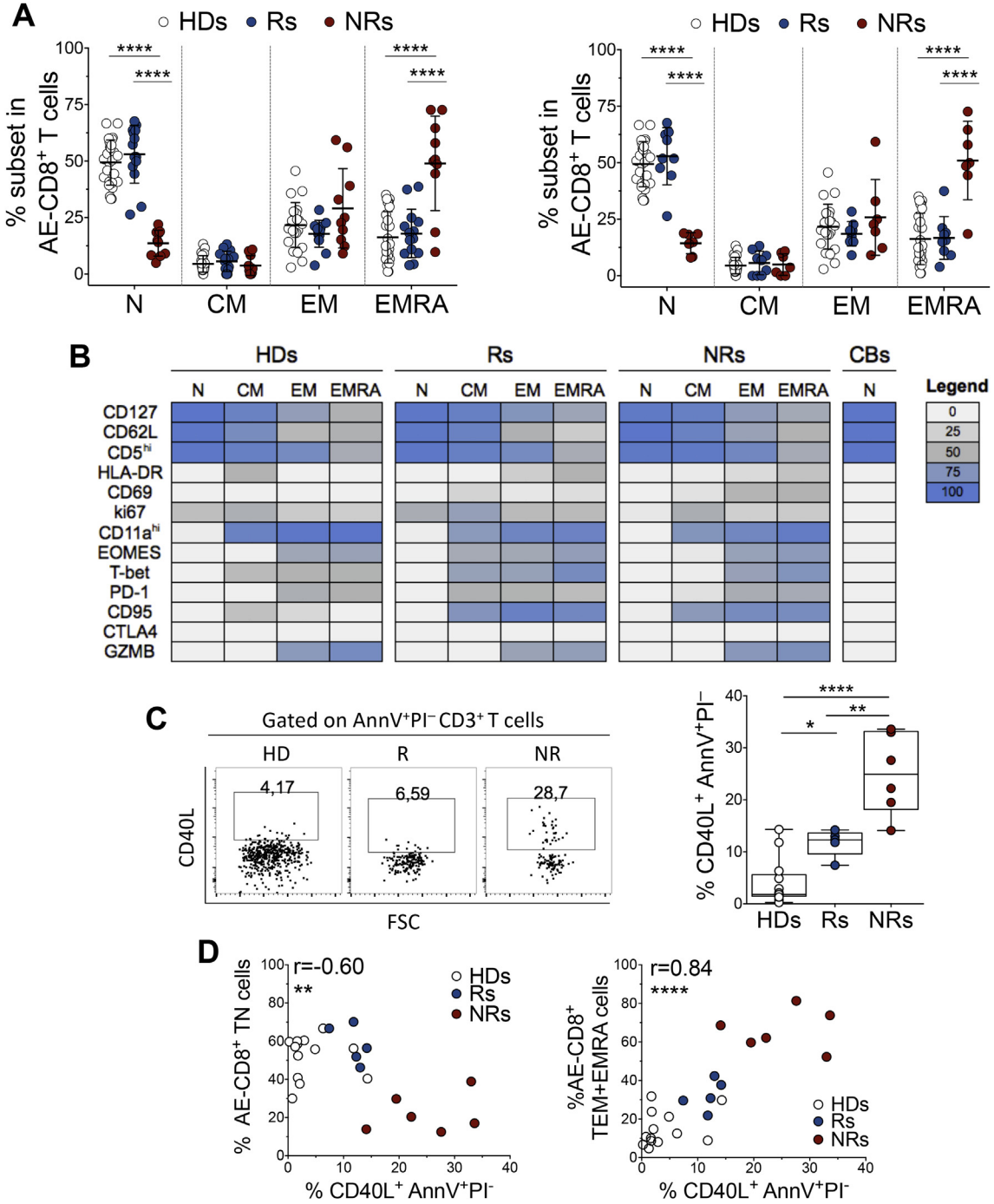

Fig. 2. Differentiation stages of AE-specific CD8$^+$ T cells in HDs and RA patients. (A) The left graph shows percentage of the indicated CD8$^+$ T cell subsets (representative FC analyses in Fig. S 2, A-C) within the pool of dextramer$^+$ CD8$^+$ T cells specific to ACTB$_{266-274}$, MYH9$_{478-486}$, MYH9$_{741-749}$, VIME$_{78-87}$, and VIME$_{225-233}$ peptides (now referred to as AE-CD8$^+$ T cells), from HDs (n = 26), Rs (n = 15), or NRs (n = 11); the right graph shows the percentages of the indicated CD8$^+$ T cell subsets within the pool of dextramer$^+$ AE-specific CD8$^+$ T cells from HDs (n = 26), and RF$^+$/ACPA$^+$ RA patients (Rs [n = 9], or NRs [n = 7]) Mean ± SD values are reported for each group; ****$p < 0.0001$ by one-way ANOVA with Tukey's multiple comparison test. (B) The heat-map represents the mean of % cells expressing the indicated markers, in cord blood cells (CBs, n = 5), or in AE-CD8$^+$ T cells from HDs (n = 15), Rs (n = 10), or NRs (n = 9): representative FC analyses and Mean ± SD values in Fig. S 2, A-D. (C) The left graph shows a representative dot plot analysis of circulating CD40L$^+$ apoptotic T cells within Annexin (Ann)V$^+$ propidium iodide (PI)$^-$ CD3$^+$ T cells from an HD, a R, or a NR; the right graph shows the percentage of CD40L$^+$ apoptotic T cells from HDs (n = 13), Rs (n = 5) and NRs (n = 6); *$p < 0.05$, **$p < 0.01$, ****$p < 0.0001$ by one-way ANOVA with Tukey's multiple comparison test. (D) The left and right graphs show the correlation between the percentage of CD40L$^+$ apoptotic T cells and frequency of AE-CD8$^+$ TN or EM + EMRA cells, respectively, from HDs (n = 13), Rs (n = 5) or NRs (n = 6); **$p < 0.01$, ****$p < 0.0001$ by Pearson correlation.

647 anti-CD8. After staining, slides were counterstained for 5 min with Hoechst (H3570, Invitrogen) and coverslipped with 60% glycerol in PBS. Confocal microscopy imaging was performed by Leica TCS-SP8X laser-scanning confocal microscope (Leica Microsystems) equipped with tunable white light laser source, 405 nm diode laser, 3 (PMT) e 2 (HyD) internal spectral detector channels. Sequential confocal images were acquired using a HC PLAPO 40× oil immersion objective (1.30 numerical aperture, Leica Microsystems) with a 1024 × 1024 image format, scan speed 400 Hz.

2.11. Statistics

Statistical analyses were performed using Graph Pad Prism version 6.0 h. To perform multiple comparisons among HDs, Rs and NRs in terms of subsets distribution, cytokine production and frequencies of Tregs, we used by one-way ANalysis Of VAriance (ANOVA) test with Tukey's multiple comparison test. The Pearson coefficient was used to measure the goodness of correlation between activated apoptotic T cells and subsets of AE-specific $CD8^+$ T cells, percentages of actTregs, and subsets of AE-specific $CD8^+$ T cells. Analysis of pZAP70 in $CD8^+$ TEM + EMRA cells from Rs and NRs was performed by unpaired Student's *t*-test, and analysis of pZAP70 at different time points was carried out with the multiple *t*-test. *In vitro* co-culture experiments of AE-specific $CD8^+$ T cells and Tregs with or without GZMB inhibitors and NKG2D neutralization Abs were analyzed with paired *t*-test or one-way Repeated Measures (RM) ANOVA with Sidak's multiple comparison test. All statistical analyses were two-tailed. Significance was set at $p < 0.05$.

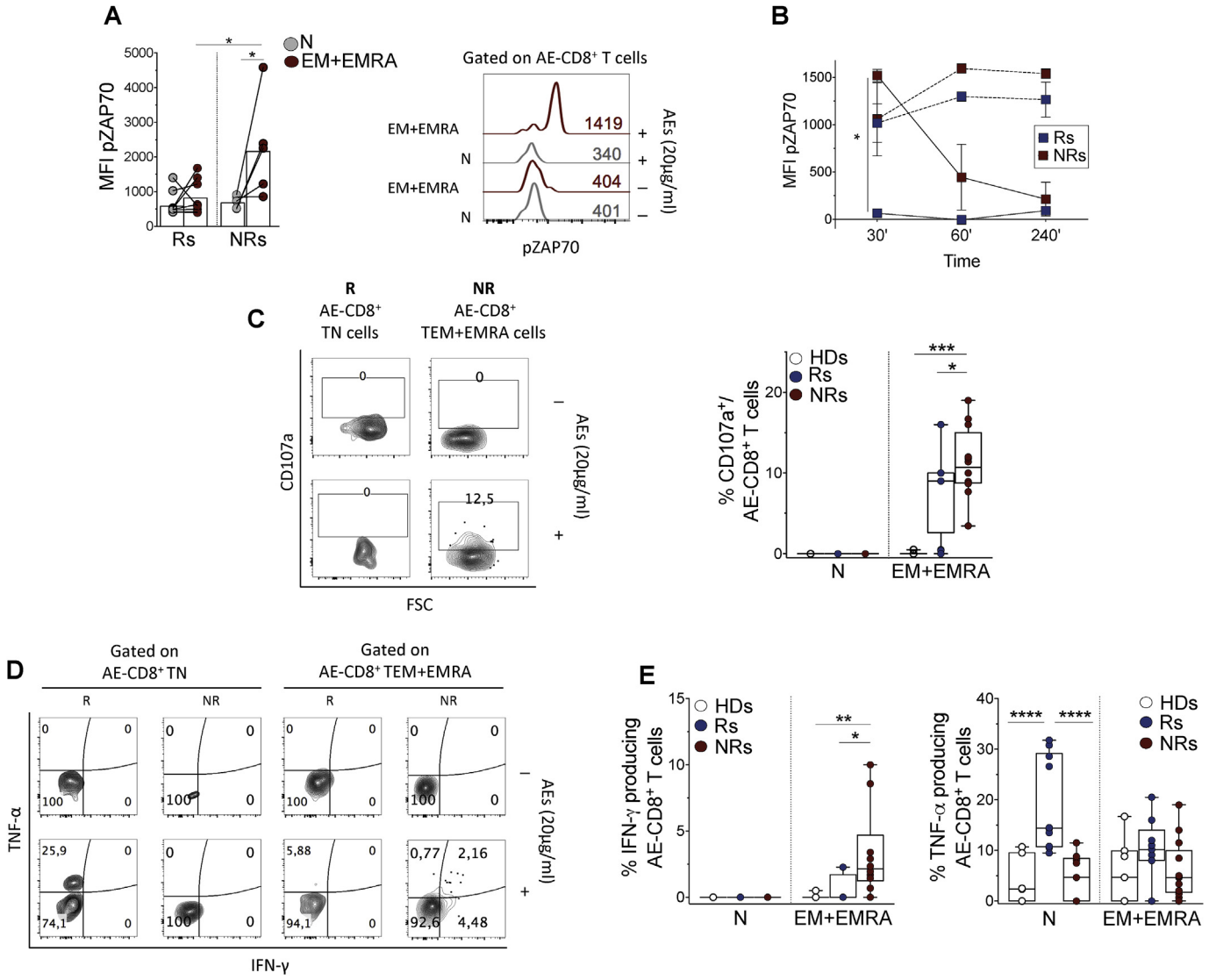

Fig. 3. Diverse functions of AE-specific $CD8^+$ T cells in Rs, and NRs. (A) The left graph shows the MFI of phosphorylated ZAP70 (pZAP70) in AE-$CD8^+$ TN or TEM + EMRA cells from Rs (n = 6) or NRs (n = 5), following PBMC stimulation or not with the pool of AEs (20 µg/mL) for 30 min; $*p < 0.05$ by the unpaired *t*-test. The right graph shows a representative analysis of pZAP70 MFI in AE-$CD8^+$ TN or TEM + EMRA cells upon PBMC stimulation (or not) with the AE pool for 30 min. (B) Time-course analysis of pZAP70 MFI in AE-$CD8^+$ T cells from Rs (n = 3) and NRs (n = 4), following PBMC stimulation with 20 µg/mL (filled line) or 100 µg/mL (dashed line) of AEs at different time points (the background [BG] was subtracted); $*p < 0.05$ by multiple *t*-test with Holm-Sidak method. (C) The left graph shows representative contour plot FC analysis of $CD107a^+$ cells both in AE-$CD8^+$ TN cells from a R and in AE-$CD8^+$ TEM + EMRA cells from a NR, after stimulation or not with 20 µg/mL of AEs (6 h); the right graph shows percentage of $CD107a^+$ cells in AE-$CD8^+$ TN or TEM + EMRA cells from HDs (n = 3), Rs (n = 9), or NRs (n = 12), upon stimulation (or not) with 20 µg/mL of AEs (the BG was subtracted). (D) Contour plot analysis of cytokines production by AE-$CD8^+$ TN or EM + EMRA cells in response to AE pool stimulation in a representative R or a representative NR. (E) IFN-γ (left graph) or TNF-α (right graph) production by AE-$CD8^+$ T cells, after stimulation with 20 µg/mL of AEs, in HDs (n = 7), Rs (n = 9) or NRs (n = 13) (the BG was subtracted). Each dot represents a single subject; $*p < 0.05$, $**p < 0.01$, $***p < 0.005$, $****p < 0.0001$ by two-way ANOVA with Sidak's multiple comparison test.

3. Data and software availability

Data source. Expression data are available at NCBI GEO: GSE105162.

4. Results

4.1. Diverse differentiation stages of AE-specific CD8$^+$ T cells in HDs, Rs, and NRs

First, we confirmed by FC analysis that autoreactive CD8$^+$ T cells specific to ACTB$_{266-274}$, MYH9$_{478-486}$, MYH9$_{741-749}$, VIME$_{78-87}$, and VIME$_{225-233}$ peptides (as detected by dextramers of HLA-A*0201 molecules complexed with relevant peptides) were significantly more abundant in HLA-A0201$^+$ RA patients who would become Rs than in those who would become NRs to anti-TNF therapy (etanercept, a recombinant fusion protein constituted by the extracellular domain of human p75 TNFR2 and the Fc region of human IgG1, or adalimumab, a human IgG1 anti-TNF antibody) (Fig. 1A-C), validating thus their usage as a unique predictive biomarker of response to TNF-α inhibitor therapies [10]. Then, more in depth FC analysis addressed to count directly *in vivo* the percentages of N (CCR7$^+$CD45RA$^+$), CM (CCR7$^+$CD45RA$^-$), EM (CCR7$^-$CD45RA$^-$), EMRA (CCR7$^-$CD45RA$^+$) cells within the pool of AE-specific CD8$^+$ T cells, in RA patients (Table 1), or in HDs, showed that they were significantly confined within the N population in HDs or in patients who would become Rs, and within the EMRA population in patients who would become NRs (Fig. 2A). The difference between NRs and Rs was also confirmed at the level of the subsets of patients resulting simultaneously positive for both rheumatoid factor (RF) and anti-citrullinated protein antibody

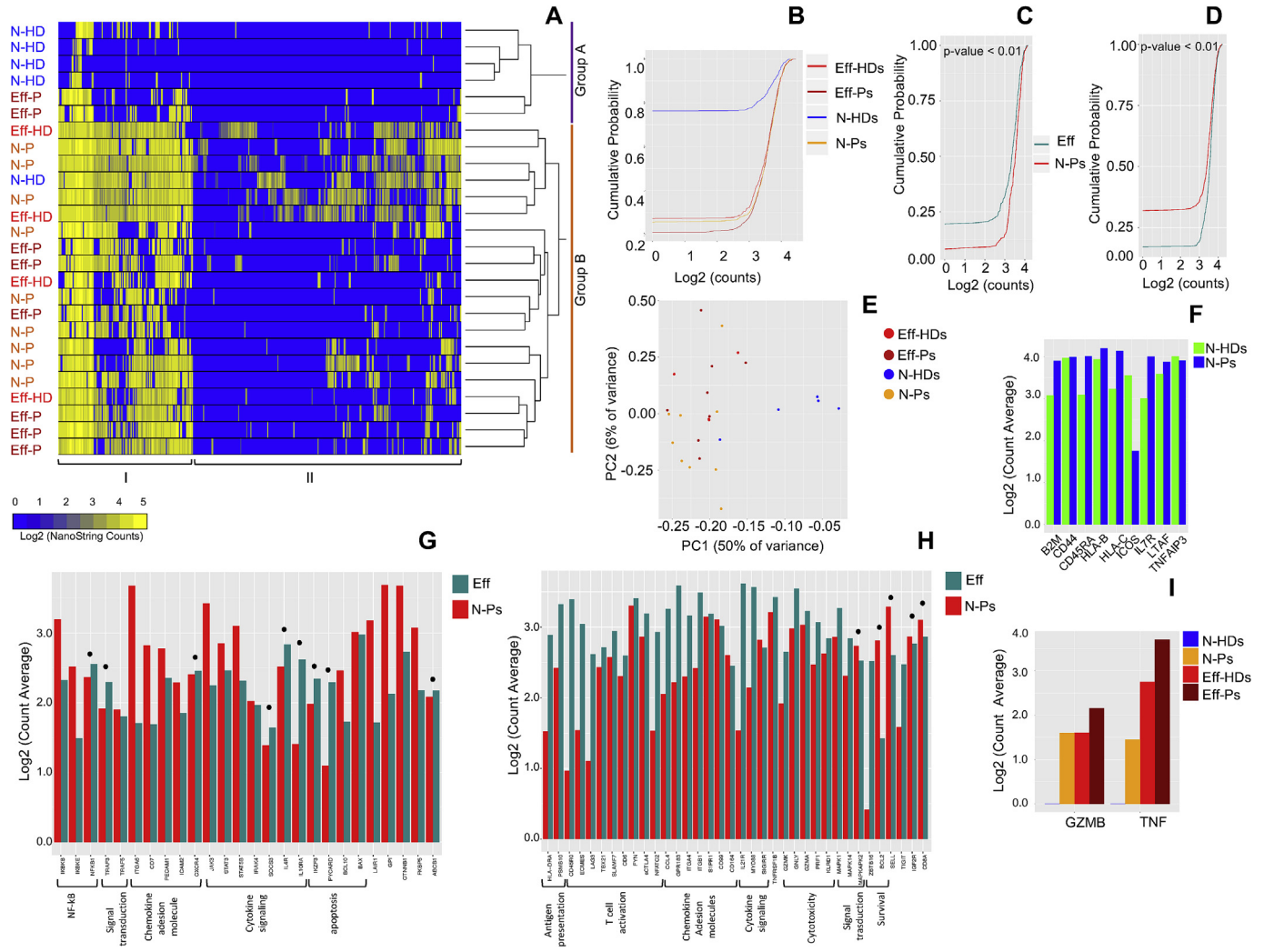

Fig. 4. Immune gene profiling of AE-specific CD8$^+$ TN or CD8$^+$ Teff cells performed with NanoString technology. (A) Samples can be broadly grouped in two clusters according to the heat-map analysis, group A (AE-specific CD8$^+$ TN cells from 5 HDs [N-HDs]) and group B (AE-specific CD8$^+$ TN cells from patients including both 4 Rs and 5 NRs [N-Ps]; AE-specific CD8$^+$ Teff cells from 4 HDs or patients including both 4 Rs and 4 NRs [Eff-HDs or Eff-Ps]). The relative abundance of transcripts is indicated by the colour (yellow, high; blue, low). (B) Uncertainty in clustering is assessed via cumulative distribution function (CDF). Results for all classes are shown: N-HDs resulted in a statistically significant separation *p-value* $< 1 \times 10^{\wedge}(-16)$ from all the other classes. (C and D) CDF values calculated for sub-clusters that were identified as having the ability to discriminate N-Ps compared with effector samples (Eff-HDs plus Eff-Ps) are shown. The two cumulative probability functions that resulted were statistically different (*p-value* < 0.01 for both of them). (E) Projection of gene expression profiles onto the first two principal components (PCs) identified by PCA replicates the separation of N-HDs from the remaining three cell types and weak separation of Eff-HDs, Eff-Ps and N-Ps detected by hierarchical clustering. Samples from different cell subtypes are designated by the same colors as in B. (F) mRNA level of the indicated genes in N-HDs and N-Ps. (G and H) Bar plot graphs show the log2 average mRNA level for genes belonging to sub-clusters I and II. On average, 19 of 26 genes in cluster I were upregulated in N-Ps (G) compared with effector cells subtype classes, whereas 30 of 38 genes in cluster II were more expressed in effector cells than in N-Ps (H). The black dots indicate genes in cluster I and II with an opposite expression level compared with the cluster expression profile. (I) mRNA expression levels of *GZMB* and *TNF-α* genes. (For interpretation of the references to color in this figure legend, the reader is referred to the Web version of this article.)

(ACPA) (Fig. 2A). No significant difference in disease activation score (as calculated by the DAS28-C reactive protein [CRP] or DAS28-erythrocyte sedimentation rate [ESR]) or disease duration [32] was observed between Rs and NRs before the start of the therapy (Table 1). No difference was observed between etanercept- and adalimumab-treated patients (data not shown). The evidence that patients who would become NRs showed a preponderant accumulation of AE-specific $CD8^+$ TEMRA cells that generally undergo contraction upon performing their effector functions, may account for the significantly lower frequency of the entire AE-specific $CD8^+$ T cell population shown in NRs, as compared with Rs (see Fig. 1A–C) [10]. AE-specific $CD8^+$ TN cells expressed additional TN cell-related markers (CD127, CD62L, $CD5^{high}$), but not those related to effector (nuclear transcription factors Eomesodermin [Eomes], nuclear transcription factor T-box [T-bet], PD-1, GZM-B) [37], anergic (CTLA-4) [9], or stem memory (CD95 and $CD11a^{high}$) [38] $CD8^+$ T cells (Fig. 2B and Fig. S2A-D). A notable number of them, but not the corresponding non-antigen-specific dextramer$^-$ TN cells or cord blood (CB) mononuclear cells, expressed the proliferation marker Ki67 significantly more in Rs than in HDs *in vivo* (Fig. 2B and Fig. S2A-D). By contrast, AE-specific $CD8^+$ T (EMRA or EM) cells co-expressed markers related to differentiated $CD8^+$ Teff cells (CD11a, CD95, Eomes, T-bet, PD-1, GZM-B), but not those related to TN cells (Fig. 2B and Fig. S2A-D). No difference was observed between etanercept- and adalimumab-treated patients (data not shown). Circulating $CD40L^+$ apoptotic T cells (previously demonstrated both to represent a major source of AEs and to enable $CD40^+$ DCs to perform stimulatory functions via the CD40L/CD40 interaction [13,15–18]) were significantly more abundant in patients who would become NRs than in those who would become Rs or in HDs, and more abundant in Rs than in HDs (Fig. 2C). The $CD40L^+$ apoptotic T cell percentage inversely correlated with the frequency of AE-specific $CD8^+$ TN cells and directly with that of AE-specific $CD8^+$ TEM/EMRA cells *in vivo*, suggesting a possible cause-and-effect relationship between these events (Fig. 2D). AE-specific $CD8^+$ T cells isolated from the SF of four RA patients with high disease activity (NRs) were represented only by AE-specific $CD8^+$ Teff (EM + EMRA) cells (Fig. S3), without any presence

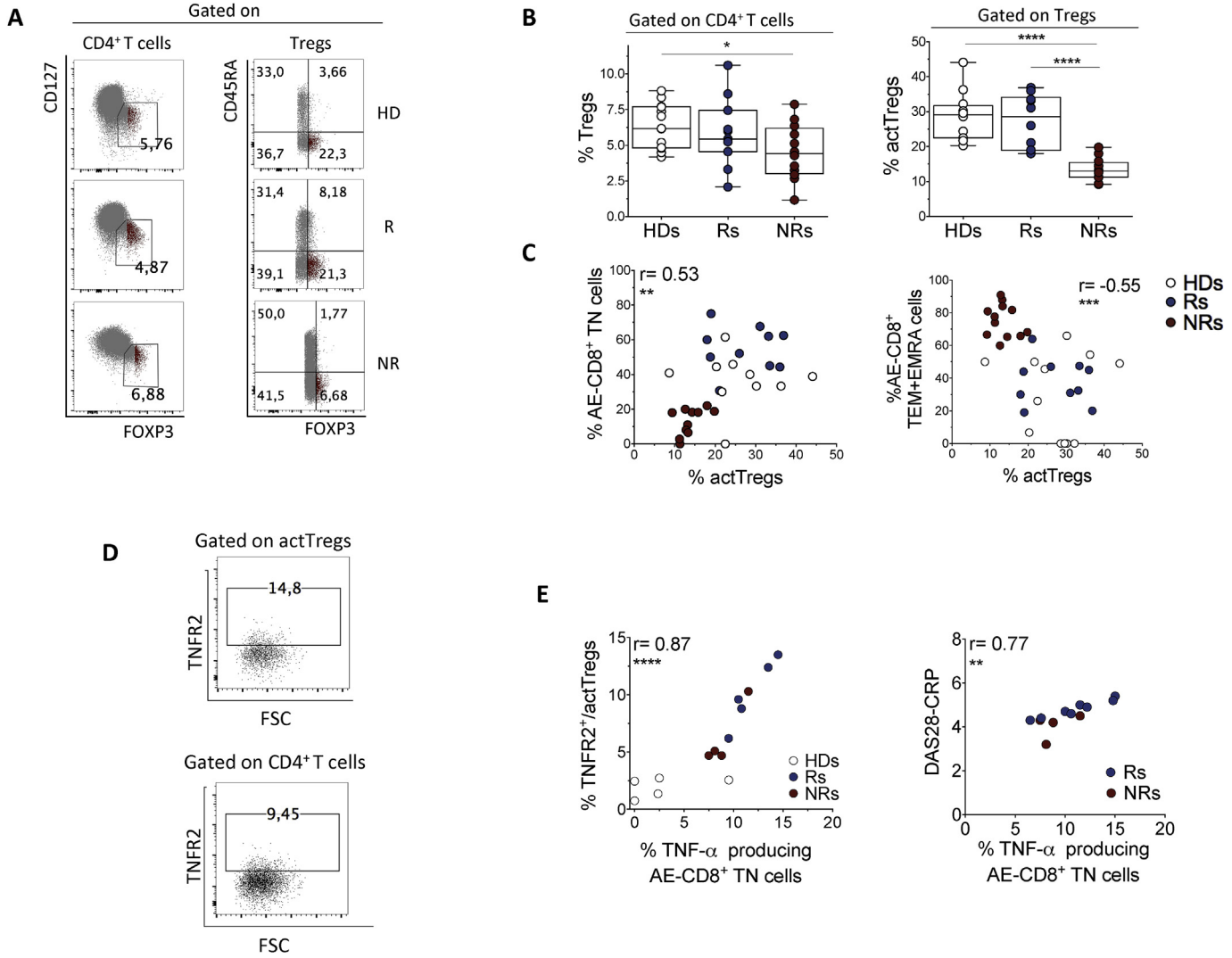

Fig. 5. Divergent correlations between activated Tregs and AE-specific $CD8^+$ TN or $CD8^+$ Teff cells. (A) Representative dot plot analysis of resting Tregs ($CD45RA^+FOXP3^{low}$) and activated (act)Tregs ($CD45RA^-FOXP3^{high}$) from an HD, a R, or a NR. (B) Percentage of Tregs (left graph) or actTregs (right graph) in HDs (n = 13), Rs (n = 10), and NRs (n = 12); $*p < 0.05$, $****p < 0.0001$ by two-tailed Mann-Whitney test. (C) Correlation between the percentage of actTregs and the frequency of AE-$CD8^+$ TN (left graph) or TEM + EMRA (right graph) cells from HDs, Rs or NRs; $**p < 0.01$, $***p < 0.005$ by the Pearson correlation. (D) The upper graph shows representative dot plot analysis of $TNFR2^+$ cells on actTregs of a RA patient; the lower graph shows representative dot plot analysis of $TNFR2^+$ cells on total $CD4^+$ T cells. (E) The left graph shows correlation between percentage of AE-$CD8^+$ TN cells producing TNF-α in response to the AEs and percentage of $TNFR2^+$ cells in actTregs in HDs (n = 5), Rs (n = 5) and NRs (n = 4); the right graph shows correlation between percentage of AE-$CD8^+$ TN cells producing TNF-α in response to the AEs and disease activity (DAS28-CRP) on baseline in Rs (n = 8) and in NRs (n = 4); $**p < 0.01$, $****p < 0.0001$ by Pearson correlation.

of their naïve counterparts (as shown in the peripheral repertoire). This data suggests that the lowest numbers of AE-specific CD8$^+$ cells shown in patients who would become NRs as compared to those who would become Rs (see Fig. 1), is also due to the possibility that AE-specific CD8$^+$ Teff (EM + EMRA) cells (see Fig. 2A), are recruited to tissues where they act as self-reactive effector cells (Fig. S3).

4.2. Diverse functions of AE-specific CD8$^+$ T cells in Rs, and NRs

AE-specific CD8$^+$ TEM + EMRA cells from patients who would become NRs showed a significantly higher TCR avidity, as detected by prompt tyrosine kinase ZAP70 phosphorylation in response to the pool of AEs, compared with both their naïve counterparts, as well as compared with the naïve or the minority of CD8$^+$ TEM + EMRA cells from Rs (Fig. 3A and B). This finding was supported by time-course analysis with two concentrations of antigen (20 and 100 μg/mL) (Fig. 3B) as well as by calculating the mean fluorescence intensity (MFI) values of dextramers binding CD8$^+$ T cells as a surrogate of TCR avidity (data not shown). Notably, the significant difference in the response to 20 μg antigen at 30 min between R and NRs, disappeared over time, likely because the 20 μg concentration is insufficient to deliver a sustained TCR stimulus providing ZAP70 phosphorylation, in contrast to the 100 μg concentration tended to maintain the difference along the time (Fig. 3B). Contextually, AE-specific CD8$^+$ TEM + EMRA cells from patients who would become NRs rapidly degranulated, in terms of CD107a (a lysosomal associated membrane protein-1) mobilization (Fig. 3C), and promptly produced IFN-γ (Fig. 3D and E) in response to AE pool significantly more than the CD8$^+$ TEM + EMRA cells from patients who would become Rs, whereas the corresponding naïve populations were virtually unable to perform these functions *ex vivo* (Fig. 3C–E). CD8$^+$ TEM + EMRA cells from Rs were not intrinsically defective, since they produced high levels of IFN-γ and efficiently degranulated in response to polyclonal stimuli (data not shown). Amazingly, high TNF-α levels were produced in response to AE pool by a notable percentage of AE-specific CD8$^+$ TN cells (significantly more in Rs than in HDs or NRs) rather than by the AE-specific TEM + EMRA cell populations (Fig. 3D and E), but not by CB cells in response to AEs or polyclonal stimuli (data not shown). These data confirm previous reports suggesting that the CD8$^+$ TN cell subset consists of a heterogeneous population of cells at various stages of development and can display a unique ability to produce TNF-α rapidly following TCR engagement, prior to differentiating into effector cells that acquire other functions such as IL-2 or IFN-γ production [39,40]. In the light of these data, from this point onward, we referred to these naïve cells as partially activated (pa)CD8$^+$ TN cells. paCD8$^+$ TN cells were unable to produce IFN-γ (Fig. 3D and E) and did not express CXCR3 (data not shown), suggesting that it is unlikely that they belong to the "memory T cells with a naive phenotype" (TMNP) population that was found to increase in frequency with age and after severe acute infections [41], but rather they might be precursors of TMNP. Non-specific (dextramer$^-$) cells were unable to respond to the AE pool (data not shown).

4.3. Gene expression profile of AE-specific CD8$^+$ TN or Teff cells

To explore whether AE-specific CD8$^+$ TN cells from HDs, and patients who would become Rs or NRs expressed different maturation stages [39,40], we performed NanoString RNA expression analysis from a tiny number (about 100 cells) of (AE-specific) CD8$^+$dextramer$^+$ TN cells or CD8$^+$ Teff (90–95% EMRA and 5–10% EM) cell populations, sorted from PBMCs of 9 HDs, 8 Rs, and 9 NRs (Fig. S4A). Clustering analysis of 401 transcripts in 26 samples, clearly displayed two distinct groups in the sample classes: group A (AE-specific CD8$^+$ TN cells from HDs [N-HDs]) which was separated from all other groups that we collectively defined as group B (AE-specific CD8$^+$ TN cells from patients including both Rs and NRs [N-Ps], and AE-specific CD8$^+$ Teff cells from HDs [Eff-HDs] or patients [Eff-Ps]) (Fig. 4A).

Moreover, genes fell into two major sub-clusters (indicated in Fig. 4A as I and II). Group A (i.e., N-HDs) was clearly characterized by downregulation of a well-defined set of 134 genes (sub-cluster I) (Fig. 4A). The CDF of the gene count probability indicated that N-Ps (without any significant difference between patients who would become Rs or NRs [data not shown]) significantly clustered nearest to AE-specific CD8$^+$ Teff cells (i.e., Eff-HDs and Eff-Ps), followed by significantly greater distance from HD naïve cells (i.e., N-HDs) (Fig. 4B), despite the fact that they had expressed a similar phenotype profile in both HDs and patients (see Fig. 2 and Fig. S2). The CDF analysis showed that two sub-clusters were composed of 26 and 38 genes, respectively (Fig. 4C and D). The former was significantly higher in N-Ps than in the cumulative effector cells (i.e., Eff-HDs plus Eff-Ps), and the latter was significantly higher in Eff than in their naïve counterparts (Fig. 4C and D). PCA unequivocally confirmed classification of N-HDs samples as a unique cell subset as detected by hierarchical clustering (Fig. 4E). Log2 average counts for genes belonging to these two sub-clusters revealed that N-Ps, in addition to the naïve genes expressed by N-HDs too (e.g., *CD45*RA, *CD127*, *CD44*) (Fig. 4F), expressed 19 of 26 genes encoding effector molecules (Fig. 4G), which were completely switched off in N-HDs, whereas 30 of 38 genes associated with effector function were more expressed in effector cells than in N-Ps (Fig. 4H). *GZMB* and *TNF-α* gene expressions, shown in the heat-map within sub-cluster II, were also detectable in N-Ps (but not in N-HDs), as well as in Eff-HDs and Eff-Ps, with different levels of expression (Fig. 4I). However, the cytotoxicity-related genes (*GZMK*, *GNLY*, *GZMA*, *PRZ1*, *KLRD1*, as well as *GZMB*) (Fig. 4H and I) taken together were more expressed by effectors than naïve cells, finding accounting for the observation that only effector cells expressed the GZM-B protein (see Fig. 2B) and displayed antigen-specific cytotoxic function (in terms of CD107a mobilization) (see Fig. 3C). The discrepancy between higher TNF-α production and lower detection of the relative mRNA in CD8$^+$ TN cells, as compared with their effector counterparts (see Figs. 3E and 4I) is not surprising, since prior studies clearly demonstrated that TNF-α production by CD8$^+$ TN cells does not require *de novo* mRNA expression, as they contain a premature TNF transcript, which, following TCR engagement, is spliced to form a mature TNF mRNA, resulting in the synthesis of TNF protein in the absence of new transcription [39,40]. Taken together, the gene expression profile analysis supported the definition of TN cells in patients (both those who would become Rs or NRs) as AE-specific paCD8$^+$ TN cells that were, however, significantly more expanded in Rs than in NRs (see Fig. 3D and E). Control analyses revealed that dextramer$^-$ naïve cells were not distinguishable between HDs and patients, but they were distinguishable from their effector counterparts in both HDs and patients (data not shown).

4.4. Tregs control AE-specific CD8$^+$ TN but not Teff cells

Phenotypic analysis of circulating Treg subsets showed that activated (act)Tregs (CD45RA^{low}FOXP3^{high}, the human Treg subpopulation expressing more stable FOXP3 expression [42]) were significantly less represented in patients who would become NRs than in Rs or HDs (Fig. 5A and B). In addition, the actTreg percentage paralleled the AE-specific CD8$^+$ TN cell frequency in a significant fashion, whereas it inversely correlated with AE-specific CD8$^+$ TEM + EMRA cell frequency (Fig. 5C). A deeper analysis confirmed that the percentage of actTregs expressing TNFR2 which, compared with conventional T cells, are known to express TNFR2 preferentially [43,44] (Fig. 5D), positively correlated with the frequency of AE-specific paCD8$^+$ TN cells producing TNF-α (Fig. 5E) (principally represented in patients who would become Rs [see Fig. 3D and E]) that, in turn, positively correlated with the disease activity score (as calculated by the DAS28-CRP) (Fig. 5E). No correlation was shown between frequency of their effector counterparts and TNFR2$^+$ actTreg percentage (data not shown). To investigate whether these events were dictated by mechanistic cause-and-effect relationships, we set up a suppression assay *in vitro*, described in

detail in Material and Methods. Highly purified ($CD4^+CD127^{low}CD25^+$) Tregs (Fig. S4B) were capable of suppressing principally the differentiation and partially the expansion of autologous AE-specific (dextramer$^+$) low avidity paCD8$^+$ TN cells (Fig. S4C) in response to relevant antigens (AEs presented by irradiated autologous (a) PBMCs as APCs [aAPCs + AEs]), as determined by the dilution of both CD45RA and CFSE expression in AE-specific CD8$^+$ TN cells (Fig. 6A). This result is consistent with the hypothesis that Tregs contribute to inhibit excessive naïve cell differentiation rather to control their proliferation, condition that ultimately results in the parallel expansion of AE-specific CD8$^+$ TN cells and actTreg *in vivo* (see Fig. 5C left graph). Amazingly, high avidity AE-specific CD8$^+$ TEM + EMRA cells (Fig. S4C) were completely resistant to Treg suppression: they efficiently proliferated in response to aAPCs + AEs, irrespective of the presence or absence of Tregs (Fig. 6B). As expected, dextramer$^-$ cells were unable to proliferate in response to aAPCs + AEs (Fig. 6C). In line with the aforementioned results, antigen-specific proliferation of AE-specific CD8$^+$ TN cells, but not of their CD8$^+$ TEM + EMRA cell counterparts, was significantly limited by Tregs at different effector/suppressor cell ratio (Fig. 6D). The same phenomenon of Treg resistance by CD8$^+$ Teff cells was observed in a non-self response setting, since the majority of CMV-specific CD8$^+$ T cells accumulated within the EM/EMRA subsets in all the HDs, Rs, and NRs tested, and showed a TCR avidity, a level of degranulation and of cytokine production in response to the relevant $CMVpp65_{495\text{-}503}$ peptide, considerably higher than those of AE-specific CD8$^+$ Teff cells (Fig. 7A-F). In addition, they (irrespective of the source they derived: i.e., Rs, NRs, or HDs) proliferated in response to the relevant CMV peptide (as indicated by the virtually complete lost of CFSE staining) and were resistant to the Treg suppression (Fig. 7G and H).

4.5. Killing Tregs by AE-specific CD8$^+$ Teff cells

Then, we questioned: Why and how are AE-specific CD8$^+$ Teff cells resistant to Tregs in a consistent percentage of RA patients? In particular, we hypothesized that the inverse correlation between AE-specific CD8$^+$ TEM + EMRA cell frequency and actTreg percentage (see Fig. 5C right graph) is unlikely dependent on the possible capacity of Tregs to suppress CD8$^+$ TEM + EMRA cells, and encouraged us to investigate whether, *vice versa*, CD8$^+$ TEM + EMRA cells may suppress Tregs by killing them. We formulated this hypothesis, on the basis of the evidences that only AE-specific CD8$^+$ TEM + EMRA (killer) cells expressed CD107a in response to AEs (see Fig. 3C) and that these CD107a$^+$ cells inversely correlated with the percentage of actTregs *in vivo* (Fig. 8A).

To provide mechanistic support to these *in vivo* findings, we set up a FC-based cytotoxicity assay (described in detail in Material and Methods) to investigate if CD8$^+$ TEM + EMRA cells, upon stimulation with aAPC + AEs, might kill allogeneic or autologous Tregs through a by-stander (indirect) mechanism [45]. Under these conditions, AE-stimulated CD8$^+$ TEM + EMRA cells (but not their non-antigen-stimulated counterparts, the AE-stimulated CD8$^+$ TN cells, or the Tregs [data

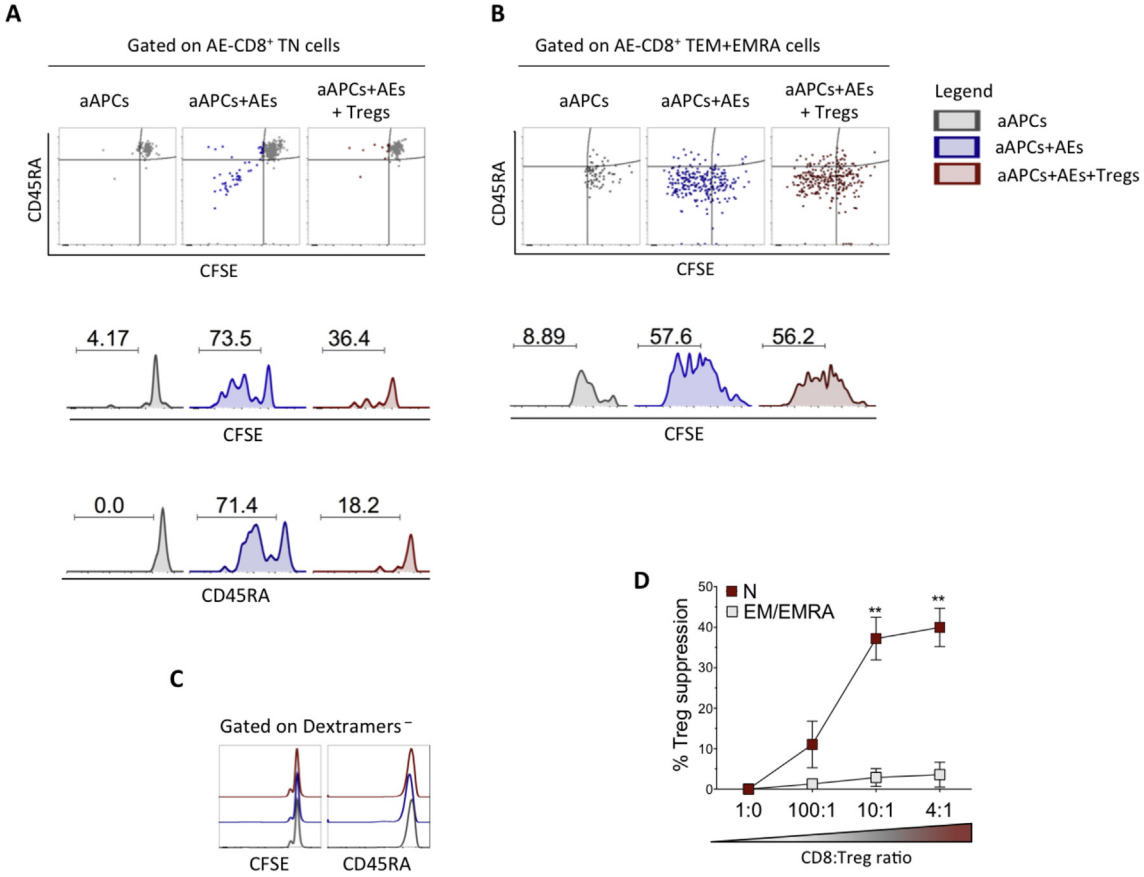

Fig. 6. Activated Tregs control AE-specific CD8$^+$ TN but not CD8$^+$ Teff cells (A and B) Representative of five suppression assays in which highly purified CFSE-stained CD8$^+$ TN cells (A) or CD8$^+$ TEM + EMRA cells (B) were stimulated with autologous (a)APCs pulsed (or not) with 20 μg/mL of AEs (aAPCs + AEs) and were co-cultured (or not) with Tregs at a CD8:Treg ratio of 10:1 for 7 days. Then cells were stained as described in Material and Methods. Dot plot analyses and the relative histograms indicate the percentage of cell proliferation (as detected by CFSE dilution) and differentiation (as detected by CD45RA downregulation) in (dextramer$^+$) AE-CD8$^+$ T cells. (C) Same experiment of panel A and B was analyzed in dextramer$^-$CD8$^+$ T cells. (D) Mean values of five independent suppression assays at different CD8:Treg ratios; %Treg suppression = (MFI CFSE-stained AE-CD8$^+$ T cells with Tregs – CFSE-stained AE-CD8$^+$ T cells without Tregs)/(MFI CFSE-stained AE-CD8$^+$ T cells with Tregs) × 100; $^{**}p < 0.01$ one-way ANOVA with Tukey's multiple comparison test.

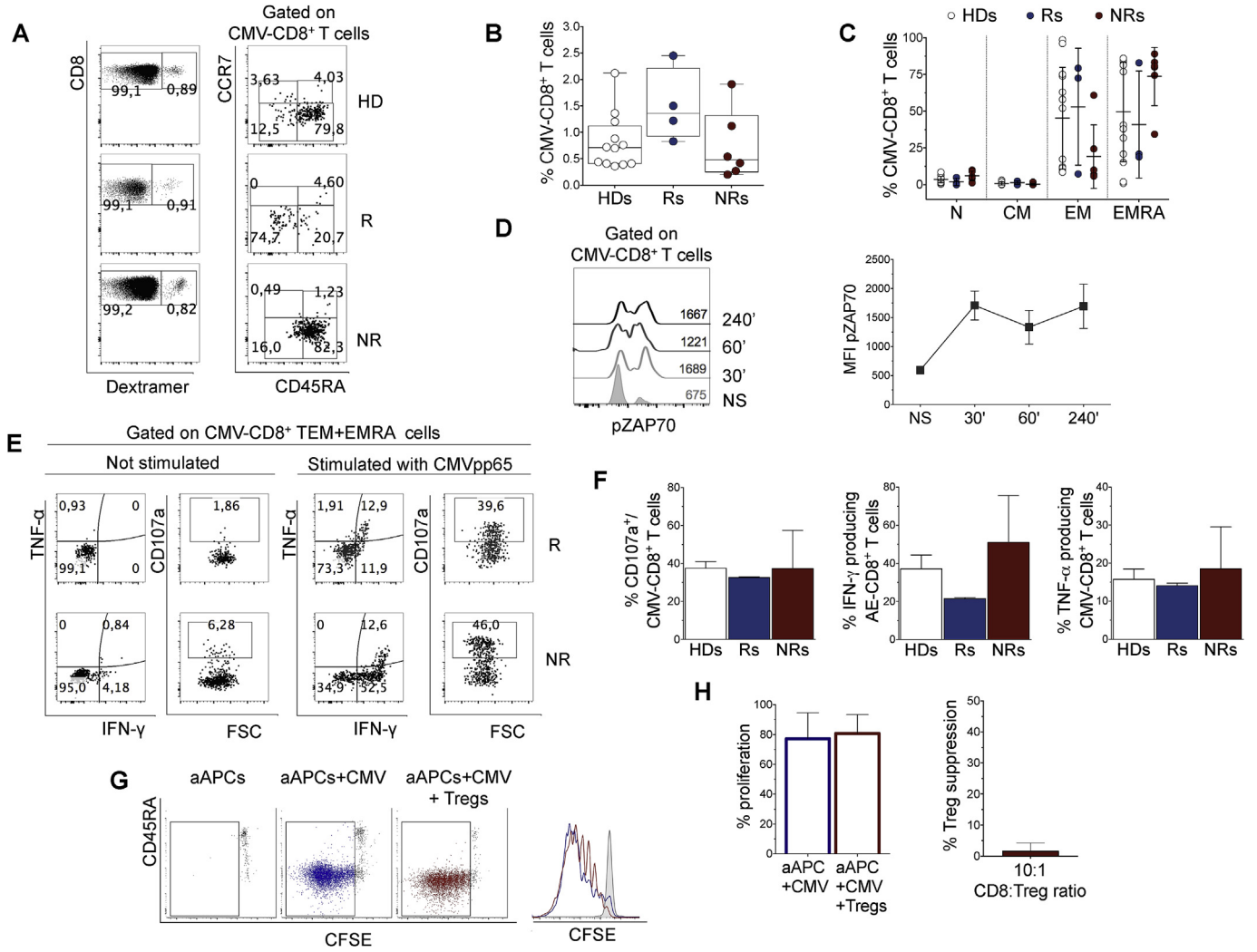

Fig. 7. Functional CMV-specific CD8$^+$ Teff cells resist Tregs. (A) Representative dot plot analyses of dextramer$^+$CD8$^+$ T cells specific to CMVpp65$_{495\text{-}503}$ (NLVP-MVATV) peptide, and of N, CM, EM and EMRA cell subsets within CMV-CD8$^+$ T cells in an HD, a R, or a NR. (B and C) Percentage of CMV-CD8$^+$ T cells (B) and distribution of N, CM, EM and EMRA cells within CMV-CD8$^+$ T cells (C) among HDs (n = 12), Rs (n = 3) or NRs (n = 6). (D) The left graph shows a representative histogram of phosphorylated ZAP70 (pZAP70) MFI in gated CMV-CD8$^+$ T cells in response to CMVpp65 peptide stimulation at different time points; the right graph shows the mean ± SD values of four independent experiments. (E) Representative dot plot FC analysis of IFN-γ$^+$, TNF-α$^+$, or CD107a$^+$ cells in gated CMV-CD8$^+$ TEM + EMRA cells from a R (upper) or a NR (lower), upon PBMC stimulation or not with 10 μg/mL CMVpp65 peptide (6 h); (F) mean ± SD values of CD107a, IFN-γ and TNF-α production in response to specific stimulation. (G) Representative suppression assay, in which highly purified CFSE-stained CD8$^+$TEM + EMRA cells were stimulated with aAPC pulsed (or not) with CMVpp65 peptide, and were co-cultured (or not) with Tregs at a CD8:Treg ratio of 10:1. Representative dot plot analysis (left graph) and the relative histograms (right graph) indicate proliferation evaluated by CFSE dilution in CMV-CD8$^+$ T cells, in the absence (blue) or in the presence (red) of Tregs. (H) Mean ± SEM values of five independent experiments indicating the percentage of proliferating CMV-CD8$^+$ T cells in the presence (red bar) or absence (blue bar) of Tregs (left graph). Mean ± SD values of five independent suppression assays (right graph); %Treg suppression = (MFI CFSE-stained AE-CD8$^+$ T cells with Tregs – CFSE-stained AE-CD8$^+$ T cells without Tregs)/(MFI CFSE-stained AE-CD8$^+$ T cells with Tregs) x 100. (For interpretation of the references to color in this figure legend, the reader is referred to the Web version of this article.)

not shown]), unveiled the expression of the activation NKG2D R [46,47] (Fig. 8B). The decreased intensity of NKG2D expression upon addition of the neutralizing anti-NKG2D antibody, which was the same both for blocking and for FC, represents a proof of the neutralization specificity (Fig. 8B). More important, the resistance of proliferating AE-specific CD8$^+$ TEM + EMRA cells to Tregs decreased upon either the addition of neutralizing anti-NKG2D antibody or the treatment of Tregs with a GZM-B inhibitor (Fig. 8C). As a consequence, Tregs acquired the capacity to suppress CD8$^+$ TEM + EMRA cells significantly, as detected by the percentage of Treg-mediated suppression of AE-specific CD8$^+$ TEM + EMRA cells (Fig. 8D). In the same system *in vitro*, the presence of AE-stimulated CD8$^+$ TEM + EMRA cells coincided with the decreased vitality of Tregs, which was significantly restored by the addition of the neutralizing anti-NKG2D mAb, thereby emphasizing the possibility that AE-specific CD8$^+$ TEM + EMRA cells can kill Tregs in a by-stander fashion (Fig. 8E). Despite the notable OX40 upregulation, actTregs did not express GZM-B as AE-specific CD8$^+$ TEM + EMRA cells *in vivo* (Fig. 8F), and were unable to kill AE-specific CD8$^+$ TEM + EMRA cells (data not shown) [48]. In addition, in an appropriate FC antigen-specific killing assay [33] (described in detail in Material and Methods), AE-specific CD8$^+$ TEM + EMRA cells directly killed AE-pulsed CFSE^{low}-stained Tregs (but not unpulsed CFSE^{high}-stained Tregs) in an antigen-specific manner, as well as conventional target cells (HLA-A0201$^+$ EBV cells derived from the JY line) at different effector/target ratios (Fig. S5). Then, we performed longitudinal analysis in 3 selected NRs, who had showed a peak of disease activation (as calculated by the DAS28-CRP) (Fig. 8G), despite the anti-TNF treatment (etanercept), to explore the interplay between actTregs and

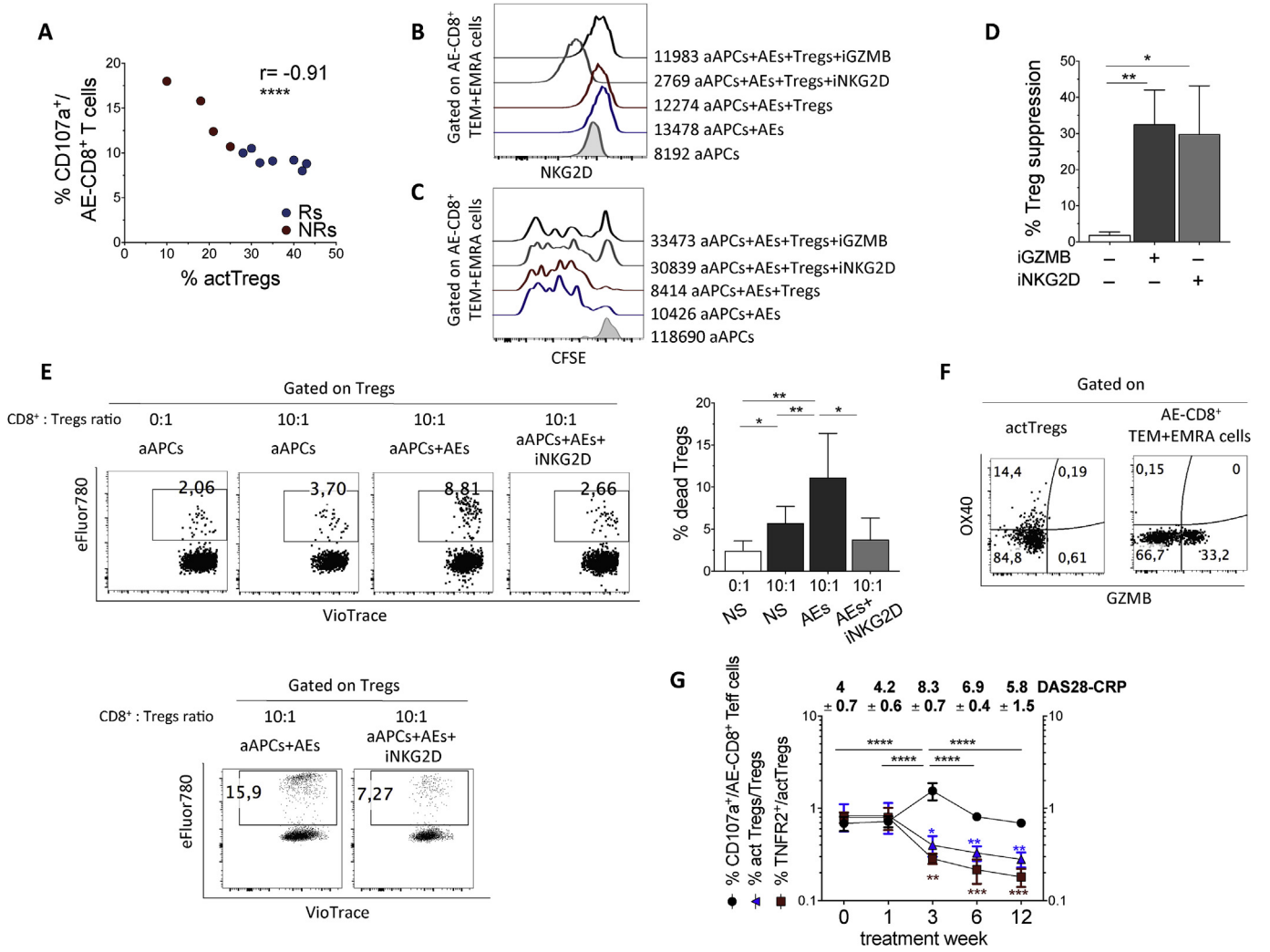

Fig. 8. CD107a$^+$ AE-specific CD8$^+$ Teff cells inversely correlate with actTregs and evade Treg suppression through a by-stander killing mechanism. (A) Correlation between the percentage of AE-CD8$^+$ T cells expressing CD107a (upon stimulation with aAPCs + AEs; the BG was subtracted) and the percentage of actTregs in Rs (n = 7) and NRs (n = 4) using Pearson coefficient, ****p < *0.0001*. (B and C) Representative experiments in which highly purified CFSE-stained CD8$^+$TEM + EMRA cells were stimulated with aAPCs + AEs and co-cultured (or not) with allogeneic Tregs (at a CD8:Treg ratio of 10:1) in the presence or absence of an inhibitor of either NKG2D (iNKG2D) or GZM-B (iGZM-B) for 7 days. Then cells were stained as described in Material and Methods. Upper panel (B) represents a histogram of NKG2D expression by AE-CD8$^+$ TEM + EMRA cells under the different indicated conditions. Lower panel (C) represents a histogram of proliferation evaluated as CFSE dilution under the different indicated conditions. (D) Mean ± SD of percentage of Treg-mediated suppression in five independent experiments in the presence or absence of iNKG2D or iGZM-B. %Treg suppression= (MFI CFSE-stained AE-CD8$^+$ T cells with Tregs – CFSE-stained AE-CD8$^+$ T cells without Tregs)/(MFI CFSE-stained AE-CD8$^+$ T cells with Tregs) × 100. *p < *0.05*, **p < *0.*01 by Paired two-tailed Student's *t*-test. (E) The left graph shows representative FC analysis of dead Tregs, as detected by the percentage of eFluor 780$^+$ cells in Tregs, alone (0:1) or co-cultured with allogeneic (upper) or autologous (lower) purified CD8$^+$TEM + EMRA cells (10:1) stimulated with aAPC + AEs in the presence or absence of iNKG2D; the right graph shows the mean of percentage of dead Tregs from five independent experiments. *p < *0.05*, **p < *0.*01 by Paired two-tailed Student's *t*-test. (F) Representative dot plot analysis of OX40 or GZM-B expression on actTregs or AE-CD8$^+$ TEM + EMRA cells. (G) Frequency of CD107a$^+$ AE-CD8$^+$ TEM + EMRA cells in response to AEs (calculated as %CD107a$^+$ AE-CD8$^+$ TEM + EMRA × %AE-CD8$^+$ TEM + EMRA) and percentage of TNFR2$^+$ actTregs or percentage of actTregs (calculated respectively as %TNFR2$^+$ on actTregs × % actTregs, and %actTregs × %Tregs respectively) during anti-TNF-α follow-up (weeks), in NRs (n = 3). The DAS28-CRP values are represented on the top of the graph. Mean ± SD are indicated; *p < *0.05*, **p < *0.01*, ***p < *0.005*, ****p < *0.*0001 by two-way ANOVA with Tukey's multiple comparison test.

AE-specific CD8$^+$ Teff cells *in vivo*. The number of AE-specific CD8$^+$ Teff (killer) cells expressing CD107a (in response to aAPCs + AEs) transiently increased in a significant fashion in relation with both the boost of disease activity and a significant decrease of both TNFR2$^+$ and actTregs, whose values were no longer back to the previous levels (Fig. 8G). Finally, in line with the killing evidences, *in situ* IHC analyses [36] showed that CD8$^+$ T cells were consistently more abundant than FOXP3$^+$ Tregs in synovial tissues derived from patients with severe RA (Fig. 9A and B). Importantly, multiplex IF staining showed that CD8$^+$ T cells expressing GZM-B directly interacted with FOXP3$^+$ Tregs (Fig. 9C), of which about 20% also expressed cleaved caspase-3 (Fig. 9C), which was not expressed by any CD8$^+$ T cells.

5. Discussion

Our findings propose two distinctive mechanisms enabling autoreactive CD8$^+$ T cells to condition Tregs to their vantage (References in [49]), and resulting hence in the expansion of either a peculiar population of autoreactive low avidity paCD8$^+$ TN cells producing high levels of TNF-α in a subset of RA patients, or polyfunctional autoreactive high-avidity CD8$^+$ Teff cells in a different subset of patients. The frequencies of both these different autoreactive T cell populations were significantly correlated with the increasing disease activity score, suggesting that both contribute to the RA pathogenesis in a different fashion. A key event contributing to initiate these different responses

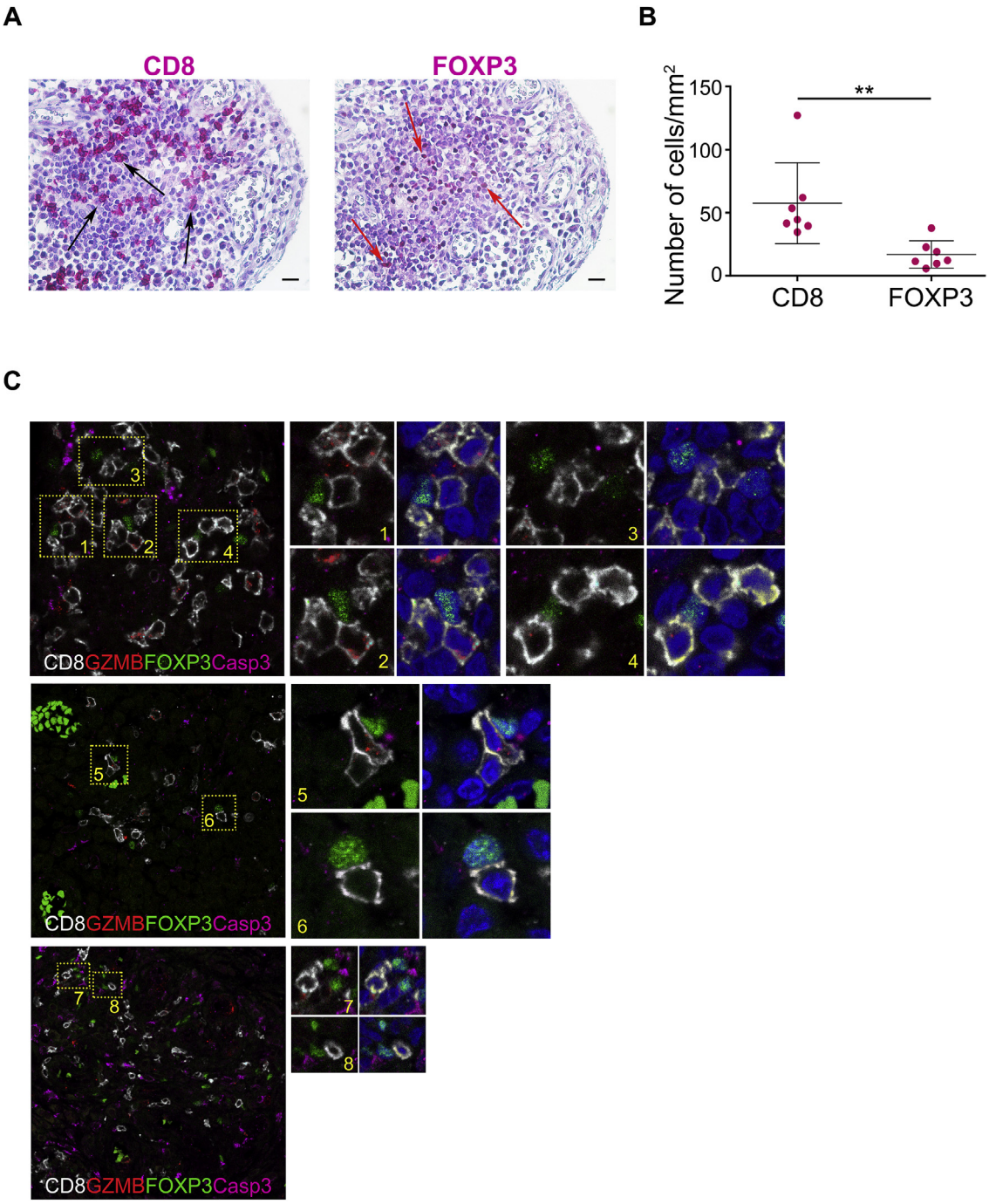

Fig. 9. CD8$^+$ T cells interact with FOXP3$^+$ Tregs in synovial tissues from patients with severe RA. (A) Representative IHC images for CD8$^+$ and FOXP3$^+$ T cells in synovial tissues are visualized with Fast Red (red) (magnification 40×). Nuclei are counter stained with haematoxylin (blue). Black and red arrows indicate CD8$^+$ and FOXP3$^+$ T cells, respectively; scale bars, 30 μm. (B) Frequency of CD8$^+$ and FOXP3$^+$ T cells within the synovial tissues from 7 RA patients. $^{**}p < 0.01$ by Paired two-tailed Student's *t*-test. (C) Quadruple co-staining of synovial tissue lesions for CD8 (white), FOXP3 (green), GZM-B (red), and cleaved Caspase-3 (magenta) is shown (magnification, 20× and 40×). Four representative scenarios of CD8$^+$ T cells interacting with FOXP3$^+$ Tregs shown within yellow rectangles are highly magnified on the right panels: CD8$^+$ T cells interacting with FOXP3$^+$ Tregs (1); GZM-B$^+$ CD8$^+$ T cells interacting with FOXP3$^+$ T regs (2, 4); CD8$^+$ T cells interacting with cleaved Caspase-3$^+$ FOXP3$^+$ Tregs (3, 6, 7, 8); GZM-B$^+$ CD8$^+$ T cells interacting with cleaved Caspase-3$^+$ FOXP3$^+$ Tregs (5). Images with nuclei (Hoechst) are shown on the rights of each panels. (For interpretation of the references to color in this figure legend, the reader is referred to the Web version of this article.)

may be related with the levels of circulating CD40L$^+$ apoptotic T cells (significantly more abundant in patients who would become NRs than in those who would become Rs), previously demonstrated to provide both antigenic (AEs) and co-activation (CD40L-dependent) signals enabling DCs to cross-prime AE-specific CD8$^+$ T cells [13,15–18]. High frequency of CD40L$^+$ apoptotic T cells may deliver the appropriate stimuli contributing to induce the full differentiation of high-avidity CD8$^+$ Teff cells, whereas low frequency of CD40L$^+$ apoptotic T cells may result in the expansion of low-avidity paCD8$^+$ TN cells [13,15–18]. Whether the different percentage of circulating CD40L$^+$ apoptotic T cells may be the result of different frequency of pre-existing pathogen-specific T cells (e.g., specific to gut or oral bacteria [27,28])

that undergo apoptosis upon performing their effector functions, is a crucial issue to investigate.

The finding that AE-specific paCD8$^+$ TN cells expressed (at transcriptional level) and promptly produced TNF-α in response to the relevant epitopes in a noticeable number of RA patients, is consistent with previous observations proposing this peculiarity as the result of a progressive activation state of TN cells [39,40]. Accordingly, our evidences showed that a considerable number of AE-specific low-avidity paCD8$^+$ TN cells expressed Ki67, produced high levels of TNF-α, and exhibited a gene expression signature that was intermediate between TN and Teff cells. These (low-avidity) paCD8$^+$ TN cells promptly producing TNF-α (but lacking other functions including the killing activity) in response to the relevant epitopes directly correlated with the disease activity score, confirming that they play a pivotal role in immunopathology in these patients by producing TNF-α, known to represent a key inflammatory cytokine involved in RA pathogenesis [19]. Importantly, they directly correlated with the percentage of circulating TNFR2$^+$ actTregs *in vivo*, and were negatively regulated by Tregs in terms of differentiation rather than proliferation *in vitro*, supporting the hypothesis proposing that TNF-α fuels TNFR2$^+$ actTregs [43,50,51], enabling the latter to, paradoxically, maintain a parallel expansion of pathogenic TNF-α-producing paCD8$^+$ TN cells, in an effort to avoid an excessive CD8$^+$ Teff cell differentiation. Ultimately, on the basis of the evidence that low avidity TNF-α$^+$ paCD8$^+$ TN cells were significantly expanded in patients who would become Rs to anti-TNF therapy as compared with NRs, we propose that they may represent a major target of both the direct effect of anti-TNF therapy and the suppression by Tregs that have been previously demonstrated to further expand upon anti-TNF treatments through multiple mechanisms in these patients [52–56]. Indeed, the beneficial effect of anti-TNF reagents has been attributed to their capacity to both dampen the TNF-α-mediated inflammatory responses [57,58], and favor the expansion of various types of Treg populations, such as transforming growth factor (TGF)-β-induced or TNFR2$^+$ Tregs through differential mechanisms, contributing ultimately to suppress the autoimmune responses [52–56]. High frequency of TNFR2$^+$ Tregs has been recently proposed as a novel biomarker predicting the beneficial effect of adalimumab in RA patients [59].

Vice versa, how autoreactive high-avidity Teff cells escape Treg control in several patients, and why these patients result NRs to therapy with any anti-TNF-α reagent, has not been completely understood so far. To explore the molecular mechanisms by which high-avidity, fully differentiated polyfunctional AE-specific CD8$^+$ Teff cells unconditionally resist Treg suppression and are not susceptible of the anti-TNF therapy, we questioned whether they escape Tregs by the capacity to kill them. This hypothesis was based on the observation that AE-specific CD8$^+$ Teff cells (as opposed to the paCD8$^+$ TN cells from Rs), not only acquired the capacity to produce IFN-γ (more than TNF-α) in response to the relevant epitopes, but also expressed high levels of GZMs (both at transcript and protein levels) and antigen-induced CD107a (killer cells) that correlated with the decrease of actTregs *in vivo*. The capacity of Treg-resistant CD8$^+$ Teff cells, which had been activated by antigen-conditioned aAPCs, to kill Tregs indirectly in an NKG2D-dependent bystander fashion *in vitro* [46], and the finding that both GZM and NKG2D inhibitors significantly restored Treg suppression through the decrease of Treg killing by CD8$^+$ Teff cells, provide a mechanistic basis for our findings *in vivo* (i.e., inverse correlation between AE-specific CD8$^+$ T killer cells and actTregs), and is consistent with the possibility that CD8$^+$ Teff cells, upon antigen stimulation by tissue-resident DCs, can indirectly counteract neighboring Tregs within inflamed tissues so as to limit excessive suppression. In addition, our results suggest a rarer eventuality, whereby Tregs acting as APCs [60–64], are directly killed by AE-specific CD8$^+$ Teff cells within inflamed tissues. The possibility that CD8$^+$ Teff cells dominate and kill Tregs in NRs *in vivo* is supported by two consistent clinical evidences. First, longitudinal study in NRs showed that a peak of AE-specific (CD107a$^+$) CD8$^+$ T killer cells coincided with a boost of severe disease activation, and a significant decrease of the actTreg values that no longer returned to the previous level, and remained persistently below the levels of AE-specific CD8$^+$ T killer cells. Second, IHC and multiplex IF imaging of inflamed synovial tissues from patients with severe RA showed that CD8$^+$ T cells were remarkably more abundant than Tregs, and that those expressing GZM-B selectively contacted FOXP3$^+$ Tregs, some of which were in an apoptotic state, validating hence the possibility that CD8$^+$ Teff cells can counteract neighboring Tregs within inflamed tissues, by killing them. These findings provide a mechanistic basis to previous clinical evidences showing that, although effector immune/inflammatory cells (including CD8$^+$ Teff cells) are accumulated in parallel with Tregs with high suppression potential in the inflamed joints of RA patients [65–67], the inflammatory process persists, and generally undergoes progressive destruction of bone and cartilage [19]. Therefore, the capacity of autoreactive high avidity CD8$^+$ Teff cells to kill Tregs would prevent the beneficial effect of anti-TNF to expand Tregs demonstrated in Rs by various groups [52–56]. The therapeutic efficacy of anti-IL6R antibody (e.g., tocilizumab) in RA patients who resulted non-responders to anti-TNF treatment [68,69], may be due to the blocking of the IL-6-dependent inhibition of Tregs [70]: whether and how the latter can then become resistant to cytotoxic cells could be an interesting topic to explore. However, because about 50% of these tocilizumab-treated patients did not achieve remission or significantly lower disease activity, our data pave the way for testing appropriate therapeutic GZM inhibitor compounds [71] in animal models and even in clinical trials in NRs to biological therapies. Additional investigation is required to determine if the combination of the killing mechanism with other molecules, related to transcripts (e.g., *CCL4*, *GPR183*, *IL-21R*) found overexpressed by AE-specific CD8$^+$ Teff cells in our study, may amplify mechanisms capable to block Tregs [72–74].

6. Conclusions

The most important facet of our findings is the evidence that high-avidity, fully differentiated AE-specific CD8$^+$ Teff cells, as we observed in patients who would become NRs to anti-TNF therapy, were completely impervious to Treg suppression. The evidence showing that CMV-specific CD8$^+$ Teff cells were also unaffected by Treg suppression suggests that the resistance to Tregs is a general mechanism employed by both self- and non-self CD8$^+$ Teff cells. We propose that CD8$^+$ Teff cells, once established in a given inflammatory milieu, can display multiple molecular strategies including the killing mechanism to counteract excessive Treg suppression. In doing so, they can preserve their effector functions, which can produce protective or detrimental effects depending on the context (e.g., infection recovery *vs.* autoimmunity). The selection of counter-regulatory mechanisms by CD8$^+$ Teff cells, during the evolutionary process, would be crucial for mounting an effective response to the aggression of infectious agents, which are by far more dangerous than autoimmunity for the survival of the human species [3]. The definition of the molecular checkpoints licensing Treg resistance by autoreactive CD8$^+$ Teff cells could be of paramount importance for the design of innovative therapeutic strategies preferentially targeting autoimmune CD8$^+$ Teff cells, in order to ultimately restore the mechanism of Treg-mediated tolerance [71,75–77]. Studies are in progress to verify whether the same mechanisms are operative in other autoimmune or allergic diseases. It would also be of extraordinary interest to investigate whether CD8$^+$ Teff cells that become exhausted in tumor or chronic infection settings lose the capacity to resist Tregs, in contrast to CD8$^+$ Teff cells with efficient effector function resolving acute viral infections.

Declarations of interest

None.

Author contributions

I·C., C.M., and A.C. performed immunology experiments (phenotypic and functional analyses of autoreactive CD8$^+$ T naïve or effector cells and regulatory T cells, purification of T cell subsets), discussed results, and contributed to the development of the study; E.C. and C·Ca. performed gene expression analysis and discussed results; D.F. and O.M. performed IHC and IF analyses and discussed results; V.D. performed IF analyses; G.V. and R.S. procured samples, recruited patients, and discussed results; G.P. performed cell sorting of autoreactive CD8$^+$ T naïve or effector cells; C·Ce. and A.Sa. provided NKG2D reagents and discussed results; A.Se. and J.S. synthesized peptides; D.R., E.M., and M.R. performed bioinformatics analysis; C.M.M. and A.M. procured biopsies of synovial tissues and discussed results; S.P. discussed results, and contributed to the development of the study; V.B. conceived the study and wrote the manuscript.

Funding

This work was supported by the following grants: Associazione Italiana per la Ricerca sul Cancro (AIRC) (progetti “Investigator Grant” [IG]-2014 id. 15199, IG-2017 id. 19939, and IG-2017 id. 19784); Ministero della Salute (Ricerca finalizzata [RF-2010-2310438 and RF 2010-2318269]); Fondazione Italiana Sclerosi Multipla (FISM) onlus (cod. 2015/R/04); Ministero dell’Istruzione, dell’Università e della Ricerca (MIUR) (PRIN 2010–2011 prot. 2010LC747T_004); Fondo per gli investimenti di ricerca di base (FIRB)-2011/13 (no. RBAP10TPXK); Istituto Pasteur Italia – Fondazione Cenci Bolognetti (grant 2014-2016); International Network Institut Pasteur, Paris – “Programmes Transversaux De Recherche” (PTR n. 20-16).

Potential referees

Antonio Lanzavecchia, Institute for Research in Biomedicine, Via Vela, 6 6500 Bellinzona, Switzerland; Dietmar Zehn, TUM School of Life Sciences Weihenstephan, Munchen, Germany; Steve Schoenberger, La Jolla Institute for Immunology, San Diego, CA; Garrisono Fathman, Division of Immunology and Rheumatology at Stanford University School of Medicine.

Acknowledgements

We thank Gabriella Girelli for providing us buffy coats of blood donors. We extend special thanks to the patients and healthy donors who participated in this study.

Appendix A. Supplementary data

Supplementary data related to this article can be found at https://doi.org/10.1016/j.jaut.2019.02.001.

References

[1] K.A. Hogquist, T.A. Baldwin, S.C. Jameson, Central tolerance: learning self-control in the thymus, Nat. Rev. Immunol. 5 (2005) 772–782.
[2] D. Mathis, C. Benoist Aire, Annu. Rev. Immunol. 27 (2009) 287–312.
[3] W. Yu, N. Jiang, P.J. Ebert, B.A. Kidd, S. Muller, P.J. Lund, et al., Clonal deletion prunes but does not eliminate self-specific alpha beta CD8(+) T lymphocytes, Immunity 42 (2015) 929–941.
[4] L.S. Walker, A.K. Abbas, The enemy within: keeping self-reactive T cells at bay in the periphery, Nat. Rev. Immunol. 2 (2002) 11–19.
[5] J.D. Fontenot, M.A. Gavin, A.Y. Rudensky, Foxp3 programs the development and function of CD4+CD25+ regulatory T cells, Nat. Immunol. 4 (2003) 330–336.
[6] S. Hori, T. Nomura, S. Sakaguchi, Control of regulatory T cell development by the transcription factor Foxp3, Science 299 (2003) 1057–1061.
[7] A.Y. Rudensky, D.J. Campbell, In vivo sites and cellular mechanisms of T reg cell-mediated suppression, J. Exp. Med. 203 (2006) 489–492.
[8] Z. Liu, M.Y. Gerner, N. Van Panhuys, A.G. Levine, A.Y. Rudensky, R.N. Germain, Immune homeostasis enforced by co-localized effector and regulatory T cells, Nature 528 (2015) 225–230.
[9] Y. Maeda, H. Nishikawa, D. Sugiyama, D. Ha, M. Hamaguchi, T. Saito, et al., Detection of self-reactive CD8(+) T cells with an anergic phenotype in healthy individuals, Science 346 (2014) 1536–1540.
[10] A. Citro, R. Scrivo, H. Martini, C. Martire, P. De Marzio, A.R. Vestri, et al., CD8+ T Cells Specific to Apoptosis-Associated Antigens Predict the Response to Tumor Necrosis Factor Inhibitor Therapy in Rheumatoid Arthritis, PLoS One 10 (2015) e0128607.
[11] D. Franceschini, P. Del Porto, S. Piconese, E. Trella, D. Accapezzato, M. Paroli, et al., Polyfunctional type-1, -2, and -17 CD8(+) T cell responses to apoptotic self-antigens correlate with the chronic evolution of hepatitis C virus infection, PLoS Pathog. 8 (2012) e1002759.
[12] F. Lolli, H. Martini, A. Citro, D. Franceschini, E. Portaccio, M.P. Amato, et al., Increased CD8+ T cell responses to apoptotic T cell-associated antigens in multiple sclerosis, J. Neuroinflammation 10 (2013) 94.
[13] P.M. Rawson, C. Molette, M. Videtta, L. Altieri, D. Franceschini, T. Donato, et al., Cross-presentation of caspase-cleaved apoptotic self antigens in HIV infection, Nat. Med. 13 (2007) 1431–1439.
[14] H. Martini, A. Citro, C. Martire, G. D'Ettorre, G. Labbadia, D. Accapezzato, et al., Apoptotic epitope-specific CD8+ T cells and interferon signaling intersect in chronic hepatitis C virus infection, J. Infect. Dis. 213 (2016) 674–683.
[15] A. Propato, G. Cutrona, V. Francavilla, M. Ulivi, E. Schiaffella, O. Landt, et al., Apoptotic cells overexpress vinculin and induce vinculin-specific cytotoxic T-cell cross-priming, Nat. Med. 7 (2001) 807–813.
[16] P. Gurung, T.A. Kucaba, T.A. Ferguson, T.S. Griffith, Activation-induced CD154 expression abrogates tolerance induced by apoptotic cells, J. Immunol. 183 (2009) 6114–6123.
[17] T.S. Griffith, T.A. Ferguson, Cell death in the maintenance and abrogation of tolerance: the five Ws of dying cells, Immunity 35 (2011) 456–466.
[18] V. Barnaba, Tuning cross-presentation of apoptotic T cells in immunopathology, Adv. Exp. Med. Biol. 785 (2013) 27–35.
[19] G.S. Firestein, Evolving concepts of rheumatoid arthritis, Nature 423 (2003) 356–361.
[20] M.C. Boissier, L. Semerano, S. Challal, N. Saidenberg-Kermanac'h, G. Falgarone, Rheumatoid arthritis: from autoimmunity to synovitis and joint destruction, J. Autoimmun. 39 (2012) 222–228.
[21] B. Nakken, L.A. Munthe, Y.T. Konttinen, A.K. Sandberg, Z. Szekanecz, P. Alex, et al., B-cells and their targeting in rheumatoid arthritis-current concepts and future perspectives, Autoimmun. Rev. 11 (2011) 28–34.
[22] N.J. Zvaifler, R.M. Steinman, G. Kaplan, L.L. Lau, M. Rivelis, Identification of immunostimulatory dendritic cells in the synovial effusions of patients with rheumatoid arthritis, J. Clin. Invest. 76 (1985) 789–800.
[23] F. Annunziato, L. Cosmi, F. Liotta, E. Maggi, S. Romagnani, Type 17 T helper cells-origins, features and possible roles in rheumatic disease, Nat. Rev. Rheumatol. 5 (2009) 325–331.
[24] A. Petrelli, F. van Wijk, CD8(+) T cells in human autoimmune arthritis: the unusual suspects, Nat. Rev. Rheumatol. 12 (2016) 421–428.
[25] M.L. Hetland, I.J. Christensen, U. Tarp, L. Dreyer, A. Hansen, I.T. Hansen, et al., Direct comparison of treatment responses, remission rates, and drug adherence in patients with rheumatoid arthritis treated with adalimumab, etanercept, or infliximab: results from eight years of surveillance of clinical practice in the nationwide Danish DANBIO registry, Arthritis Rheum. 62 (2010) 22–32.
[26] J.S. Smolen, M.E. Weinblatt, S. Sheng, Y. Zhuang, B. Hsu Sirukumab, A human anti-interleukin-6 monoclonal antibody: a randomised, 2-part (proof-of-concept and dose-finding), phase II study in patients with active rheumatoid arthritis despite methotrexate therapy, Ann. Rheum. Dis. 73 (2014) 1616–1625.
[27] H.J. Wu, Ivanov II, J. Darce, K. Hattori, T. Shima, Y. Umesaki, et al., Gut-residing Segmented Filamentous Bacteria Drive Autoimmune Arthritis via T Helper 17 Cells, Immunity vol. 32, (2010) 815–827.
[28] G. Hajishengallis, Periodontitis: From microbial immune subversion to systemic inflammation, Nat. Rev. Immunol. 15 (2015) 30–44.
[29] M.F. Konig, J.T. Giles, P.A. Nigrovic, F. Andrade, Antibodies to native and citrullinated RA33 (hnRNP A2/B1) challenge citrullination as the inciting principle underlying loss of tolerance in rheumatoid arthritis, Ann. Rheum. Dis. 75 (2016) 2022–2028.
[30] I.B. McInnes, G. Schett, The pathogenesis of rheumatoid arthritis, N. Engl. J. Med. 365 (2011) 2205–2219.
[31] M.L.L. Prevoo, M.A. Van'T Hof, H.H. Kuper, M.A. Van Leeuwen, L.B.A. Van De Putte, P.L.C.M. Van Riel, Modified disease activity scores that include twenty-eight-joint counts development and validation in a prospective longitudinal study of patients with rheumatoid arthritis, Arthritis Rheum. 38 (1995) 44–48.
[32] A.M. van Gestel, C.J. Haagsma, P.L. van Riel, Validation of rheumatoid arthritis improvement criteria that include simplified joint counts, Arthritis Rheum. 41 (1998) 1845–1850.
[33] A. Noto, P. Ngauv, L. Trautmann, Cell-based flow cytometry assay to measure cytotoxic activity, JoVE : JoVE (2013) e51105.
[34] D. Waggott, K. Chu, S. Yin, B.G. Wouters, F.F. Liu, P.C. Boutros, NanoStringNorm: an extensible R package for the pre-processing of NanoString mRNA and miRNA data, Bioinformatics 28 (2012) 1546–1548.
[35] T. Galili, dendextend: an R package for visualizing, adjusting and comparing trees of hierarchical clustering, Bioinformatics 31 (2015) 3718–3720.
[36] O. Melaiu, M. Mina, M. Chierici, R. Boldrini, G. Jurman, P. Romania, et al., PD-L1 is a therapeutic target of the bromodomain inhibitor JQ1 and, combined with HLA class I, a promising prognostic biomarker in neuroblastoma, Clin. Cancer Res. : Off. J. Am. Assoc. Cancer Res. 23 (2017) 4462–4472.
[37] E.J. Wherry, M. Kurachi, Molecular and cellular insights into T cell exhaustion, Nat.

Rev. Immunol. 15 (2015) 486–499.
[38] L. Gattinoni, E. Lugli, Y. Ji, Z. Pos, C.M. Paulos, M.F. Quigley, et al., A human memory T cell subset with stem cell-like properties, Nat. Med. 17 (2011) 1290–1297.
[39] M.A. Brehm, K.A. Daniels, R.M. Welsh, Rapid production of TNF-alpha following TCR engagement of naive CD8 T cells, J. Immunol. 175 (2005) 5043–5049.
[40] Y. Yang, J.F. Chang, J.R. Parnes, C.G. Fathman, T cell receptor (TCR) engagement leads to activation-induced splicing of tumor necrosis factor (TNF) nuclear pre-mRNA, J. Exp. Med. 188 (1998) 247–254.
[41] V. Pulko, J.S. Davies, C. Martinez, M.C. Lanteri, M.P. Busch, M.S. Diamond, et al., Human memory T cells with a naive phenotype accumulate with aging and respond to persistent viruses, Nat. Immunol. 17 (2016) 966–975.
[42] M. Miyara, Y. Yoshioka, A. Kitoh, T. Shima, K. Wing, A. Niwa, et al., Functional delineation and differentiation dynamics of human CD4+ T cells expressing the FoxP3 transcription factor, Immunity 30 (2009) 899–911.
[43] X. Chen, J.J. Subleski, H. Kopf, O.M. Howard, D.N. Mannel, J.J. Oppenheim, Cutting edge: expression of TNFR2 defines a maximally suppressive subset of mouse CD4+CD25+FoxP3+ T regulatory cells: applicability to tumor-infiltrating T regulatory cells, J. Immunol. 180 (2008) 6467–6471.
[44] M. Nagar, J. Jacob-Hirsch, H. Vernitsky, Y. Berkun, S. Ben-Horin, N. Amariglio, et al., TNF activates a NF-kappaB-regulated cellular program in human CD45RA- regulatory T cells that modulates their suppressive function, J. Immunol. 184 (2010) 3570–3581.
[45] A. Lanzavecchia, Is the T-cell receptor involved in T-cell killing? Nature 319 (1986) 778–780.
[46] T. Chu, A.J. Tyznik, S. Roepke, A.M. Berkley, A. Woodward-Davis, L. Pattacini, et al., Bystander-activated memory CD8 T cells control early pathogen load in an innate-like, NKG2D-dependent manner, Cell Rep. 3 (2013) 701–708.
[47] S. Bauer, V. Groh, J. Wu, A. Steinle, J.H. Phillips, L.L. Lanier, et al., Activation of NK cells and T cells by NKG2D, a receptor for stress-inducible MICA, Science 285 (1999) 727–729.
[48] S. Koristka, M. Cartellieri, C. Arndt, A. Feldmann, K. Topfer, I. Michalk, et al., Cytotoxic response of human regulatory T cells upon T-cell receptor-mediated activation: a matter of purity, Blood Canc. J. 4 (2014) e199.
[49] L.S. Walker, Regulatory T cells overturned: the effectors fight back, Immunology 126 (2009) 466–474.
[50] X. Chen, J.J. Oppenheim, Contrasting effects of TNF and anti-TNF on the activation of effector T cells and regulatory T cells in autoimmunity, FEBS Lett. 585 (2011) 3611–3618.
[51] B. Zaragoza, X. Chen, J.J. Oppenheim, A. Baeyens, S. Gregoire, D. Chader, et al., Suppressive activity of human regulatory T cells is maintained in the presence of TNF, Nat. Med. 22 (2016) 16–17.
[52] D.X. Nguyen, M.R. Ehrenstein, Anti-TNF drives regulatory T cell expansion by paradoxically promoting membrane TNF-TNF-RII binding in rheumatoid arthritis, J. Exp. Med. 213 (2016) 1241–1253.
[53] S. Nadkarni, C. Mauri, M.R. Ehrenstein, Anti-TNF-alpha therapy induces a distinct regulatory T cell population in patients with rheumatoid arthritis via TGF-beta, J. Exp. Med. 204 (2007) 33–39.
[54] J. Biton, L. Semerano, L. Delavallee, D. Lemeiter, M. Laborie, G. Grouard-Vogel, et al., Interplay between TNF and regulatory T cells in a TNF-driven murine model of arthritis, J. Immunol. 186 (2011) 3899–3910.
[55] Q. Zhang, F. Cui, L. Fang, J. Hong, B. Zheng, J.Z. Zhang, TNF-alpha impairs differentiation and function of TGF-beta-induced Treg cells in autoimmune diseases through Akt and Smad 3 signaling pathway, J. Mol. Cell Biol. 5 (2013) 85–98.
[56] M.R. Ehrenstein, J.G. Evans, A. Singh, S. Moore, G. Warnes, D.A. Isenberg, et al., Compromised function of regulatory T cells in rheumatoid arthritis and reversal by anti-TNFalpha therapy, J. Exp. Med. 200 (2004) 277–285.
[57] D. Brenner, H. Blaser, T.W. Mak, Regulation of tumour necrosis factor signalling: live or let die, Nat. Rev. Immunol. 15 (2015) 362–374.
[58] R. Byng-Maddick, M.R. Ehrenstein, The impact of biological therapy on regulatory T cells in rheumatoid arthritis, Rheumatology 54 (2015) 768–775.
[59] D.X. Nguyen, A. Cotton, L. Attipoe, C. Ciurtin, C.J. Dore, M.R. Ehrenstein, Regulatory T cells as a biomarker for response to adalimumab in rheumatoid arthritis, J. Allergy Clin. Immunol. 142 (2018) 978–980 e9.
[60] V. Barnaba, C. Watts, M. de Boer, P. Lane, A. Lanzavecchia, Professional presentation of antigen by activated human T cells, Eur. J. Immunol. 24 (1994) 71–75.
[61] A. Franco, M. Paroli, U. Testa, R. Benvenuto, C. Peschle, F. Balsano, et al., Transferrin receptor mediates uptake and presentation of hepatitis B envelope antigen by T lymphocytes, J. Exp. Med. 175 (1992) 1195–1205.
[62] J. Helft, A. Jacquet, N.T. Joncker, I. Grandjean, G. Dorothee, A. Kissenpfennig, et al., Antigen-specific T-T interactions regulate CD4 T-cell expansion, Blood 112 (2008) 1249–1258.
[63] S. Salemi, A.P. Caporossi, L. Boffa, M.G. Longobardi, V. Barnaba, HIVgp120 activates autoreactive CD4-specific T cell responses by unveiling of hidden CD4 peptides during processing, J. Exp. Med. 181 (1995) 2253–2257.
[64] J.M. LaSalle, F. Toneguzzo, M. Saadeh, D.E. Golan, R. Taber, D.A. Hafler, T-cell presentation of antigen requires cell-to-cell contact for proliferation and anergy induction. Differential MHC requirements for superantigen and autoantigen, J. Immunol. 151 (1993) 649–657.
[65] M. Mottonen, J. Heikkinen, L. Mustonen, P. Isomaki, R. Luukkainen, O. Lassila, CD4+ CD25+ T cells with the phenotypic and functional characteristics of regulatory T cells are enriched in the synovial fluid of patients with rheumatoid arthritis, Clin. Exp. Immunol. 140 (2005) 360–367.
[66] A. Rissiek, I. Baumann, A. Cuapio, A. Mautner, M. Kolster, P.C. Arck, et al., The expression of CD39 on regulatory T cells is genetically driven and further upregulated at sites of inflammation, J. Autoimmun. 58 (2015) 12–20.
[67] G.J. Walter, H.G. Evans, B. Menon, N.J. Gullick, B.W. Kirkham, A.P. Cope, et al., Interaction with activated monocytes enhances cytokine expression and suppressive activity of human CD4+CD45ro+CD25+CD127(low) regulatory T cells, Arthritis Rheum. 65 (2013) 627–638.
[68] P. Emery, E. Keystone, H.P. Tony, A. Cantagrel, R. van Vollenhoven, A. Sanchez, et al., IL-6 receptor inhibition with tocilizumab improves treatment outcomes in patients with rheumatoid arthritis refractory to anti-tumour necrosis factor biologicals: results from a 24-week multicentre randomised placebo-controlled trial, Ann. Rheum. Dis. 67 (2008) 1516–1523.
[69] A. Kaneko, Tocilizumab in rheumatoid arthritis: efficacy, safety and its place in therapy, Therapeutic Adv. Chronic Disease 4 (2013) 15–21.
[70] C. Pasare, R. Medzhitov, Toll pathway-dependent blockade of CD4+CD25+ T cell-mediated suppression by dendritic cells, Science 299 (2003) 1033–1036.
[71] M. Marcet-Palacios, C. Ewen, E. Pittman, B. Duggan, K. Carmine-Simmen, R.P. Fahlman, et al., Design and characterization of a novel human Granzyme B inhibitor, Protein Eng. Des. Sel. : PEDS 28 (2015) 9–17.
[72] J.Y. Liu, F. Li, L.P. Wang, X.F. Chen, D. Wang, L. Cao, et al., CTL- vs Treg lymphocyte-attracting chemokines, CCL4 and CCL20, are strong reciprocal predictive markers for survival of patients with oesophageal squamous cell carcinoma, BJC (Br. J. Cancer) 113 (2015) 747–755.
[73] K. Attridge, C.J. Wang, L. Wardzinski, R. Kenefeck, J.L. Chamberlain, C. Manzotti, et al., IL-21 inhibits T cell IL-2 production and impairs Treg homeostasis, Blood 119 (2012) 4656–4664.
[74] F. Wanke, S. Moos, A.L. Croxford, A.P. Heinen, S. Graf, B. Kalt, et al., EBI2 is highly expressed in multiple sclerosis lesions and promotes early CNS migration of encephalitogenic CD4 T cells, Cell Rep. 18 (2017) 1270–1284.
[75] R.R. Caspi, Immunotherapy of autoimmunity and cancer: the penalty for success, Nat. Rev. Immunol. 8 (2008) 970–976.
[76] Q. Zhang, D.A. Vignali, Co-stimulatory and Co-inhibitory pathways in autoimmunity, Immunity 44 (2016) 1034–1051.
[77] R.S. Liblau, F.S. Wong, L.T. Mars, P. Santamaria, Autoreactive CD8 T cells in organ-specific autoimmunity: emerging targets for therapeutic intervention, Immunity 17 (2002) 1–6.